Single cell photoacoustic microscopy: a review

Eric M. Strohm, Michael J. Moore, Michael C. Kolios

***Abstract*—Photoacoustic imaging has experienced exponential growth over the past decade, with many applications in biomedicine. One application ideally suited to the analysis of single cells is photoacoustic microscopy (PAM). Using PAM, detailed sub-micrometer resolution images of single cells can be produced, with contrast dependent primarily on the optical absorption properties of the cell. A multi-wavelength approach for targeting specific endogenous or exogenous chromophores can enhance cellular detail and resolve single organelles with contrast not possible with traditional optical microscopy. A quantitative analysis of the photoacoustic signals acquired from single cells can provide insight into their anatomical, biomechanical and functional properties. This information can be used to identify specific cells, or to enhance the understanding of biological processes at the single cell level. This comprehensive review on PAM covers recent advances in high resolution PAM, signal processing methods and potential clinical applications targeting single cells in-vitro and in-vivo.**

***Index Terms*—Photoacoustic effect, photoacoustic imaging, photoacoustic microscopy.**

1. INTRODUCTION

"MR. Bell, if you hear what I say, come to the window and wave your hat." – Sumner Tainter, 1880 [1].

The production of acoustic waves by a source of light was first demonstrated by Alexander Graham Bell in 1880. Bell discovered that spoken words used to modulate the intensity of a light source could be reproduced if the light beam was subsequently focused on to a thin diaphragm [1]. Bell and his assistant, Sumner Tainter, used this phenomenon to transmit their voice across a 220 meter distance, demonstrating the first practical use of the photophone. The production of sound from light, which came to be known as the photoacoustic effect (or optoacoustic effect), was briefly investigated in solids, liquids, and gases [2]. After seminal works by Bell [1], [2], Tyndall [3], and Röntgen [4], research fell dormant for several decades until the 1930's when an application was found in gas spectroscopy [5]. Research in gas spectroscopy dominated until Rosencwaig provided a second renewal of interest by demonstrating photoacoustic spectroscopy of solids in the 1970's [6], [7]; however, it was his studies on biological material that paved the way for modern day biological photoacoustics [8]. Research in biomedical photoacoustics has experienced significant growth over the past decade, with demonstrated applications in diagnostic imaging at both the single cell and tissue structure level in-vitro and in-vivo.

[T]E.M. Strohm, M.J. Moore, M.C. Kolios, Department of Physics, Ryerson University, Toronto, ON, M5B2K3 Canada. (e-mail: mkolios@ryerson.ca).

A. The Photoacoustic Effect

A brief overview of photoacoustic theory is given here. Interested readers may refer to [9]–[18] for rigorous derivations and descriptions. The photoacoustic effect is initiated when an optically absorbing object is irradiated by a temporally modulated source of light. Photon absorption and subsequent non-radiative relaxation by chromophores induces a rapid rise in temperature within the sample. If a pulsed laser with pulse duration shorter than the sample thermal and stress confinement times is used, then no thermal energy is exchanged with the surroundings, and energy deposition occurs on timescales shorter than those needed for mechanical displacements causing strain within the sample to occur [19]. This isochoric heating raises the pressure within the sample by $\Delta p = \Gamma \mu_a F$, where Γ is the Grüneisen parameter, μ_a is the optical absorption coefficient, and F is the incident laser fluence [14]. This pressure rise induces a thermoelastic expansion and the emission of a pressure wave called a photoacoustic wave. The broadband photoacoustic wave is encoded with information pertaining to the geometrical properties of the absorbing structures, and is governed by the inhomogeneous wave equation

$$\left(\nabla^2 - \frac{1}{v_s^2}\frac{\partial}{\partial t}\right)p = -\frac{\beta}{C_p}\frac{\partial H}{\partial t}, \quad (1)$$

where β is the thermal expansion coefficient of the sample, C_p is the specific heat capacity, and H is a function which describes the heating of the sample in time and space [20]–[22]. The closed form solution to equation (1) has been derived for simple geometries including the half-plane, infinite and finite cylinder, ellipsoid, and sphere [20], [23]–[27].

2. PHOTOACOUSTIC MICROSCOPY (PAM)

Acoustic and photoacoustic waves are both mechanical waves; the only difference lies in the method used for their generation. The acoustic microscope, which typically uses ultrasound with frequencies greater than 100 MHz, was first developed in the 1970's [28]; shortly thereafter, the feasibility of photoacoustics on a microscopic scale was first demonstrated by Wickramasinghe et al. in 1978 [12]. An acoustic microscope outfitted with an 840 MHz central frequency transducer was modified to include an objective lens along the acoustic axis of the transducer. A 1064 nm Nd:YAG laser focused along the optical path was used for sample irradiation, and emitted photoacoustic waves were acquired with the high-frequency transducer [12]. Variations of the photoacoustic microscopy (PAM) technique were quickly adopted and used for subsurface imaging and flaw detection in metals and ceramics [12], [29]–[33], spectroscopy

in ex vivo biological specimens [34], [35], and much later in vivo using both exogenous and endogenous contrast agents [36].

There are two main configurations for PAM as shown in figure 2.1: reflection mode, where the illumination source and ultrasonic detector are on the same side of the sample; and transmission mode, where they are on opposing sides [37], [38]. The technique is further subdivided into optical resolution (OR-PAM) and acoustic resolution (AR-PAM) based on what drives the resolution of the imaging method: the diameter of the laser beam (OR-PAM) or the transducer focal spot (AR-PAM). In OR-PAM, the incident light is focused to a diffraction limited spot on the sample, which provides a spatially constrained acoustic source and dictates the lateral resolution of the system [39], [40]. In AR-PAM a larger optical spot is used (or the light beam diffuses within the sample), and thus the lateral resolution is defined by the transducer focal spot, which itself is inversely related to the central frequency of the transducer. The axial resolution in both setups is defined by the transducer geometrical focusing and the inverse of the transducer bandwidth [41]. For transducers in the 20-100 MHz range, the axial resolution in OR-PAM is poor compared to the lateral resolution; however, the AR-PAM lateral and axial resolutions can be comparable depending on the transducer design [42].

The laser pulse width should be selected to ensure that it is less than the thermal and stress confinement times of the sample. If the pulse width is larger than these confinement times, the amplitude of the emitted photoacoustic wave is reduced and higher frequencies will not be generated [22], [43]. For micrometer-sized objects such as single cells, or when broadband spectral analysis is required, pulse widths < 1 ns should be used for optimal photoacoustic signal generation.

When using transducers with central frequencies less than 100 MHz, OR-PAM is best suited for probing thin tissue slices or single cells and AR-PAM is better for probing tissues at depths where the focused optical beams scatter and become diffuse [44]. A good overview of the advantages and disadvantages of OR-PAM, AR-PAM and the theoretical considerations of resolution and attenuation can be found in [45]. When using transducers with central frequencies near 1000 MHz, acoustic attenuation in the coupling fluid and sample limits the photoacoustic interrogation depth to a few cell layers or less. However, the wide bandwidths of these ultra-high frequency transducers provide enhanced axial resolution and enable a quantitative analysis of the emitted photoacoustic signals that is not possible in low frequency or narrow bandwidth systems.

Single cell PAM measurements depend primarily upon the choice of transducer central frequency. Therefore the review is split into three sections: 1) photoacoustic imaging using ultrasound detection frequencies < 200 MHz (OR-PAM, where resolution is achieved through focusing the laser to a small spot), 2) photoacoustic imaging using ultrasound detection frequencies at 1000 MHz (hybrid OR-PAM and AR-PAM, where the optical and acoustic resolutions are similar) and 3) a quantitative analysis of photoacoustic signals and of the photoacoustic signal frequency spectrum.

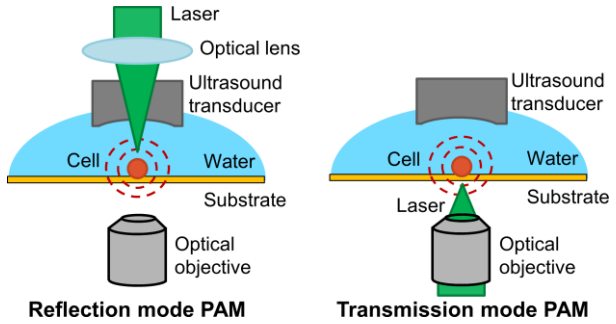

Figure 2.1: Schematic representation of different PAM setups: (Left) reflection mode, where the laser travels through or around the transducer, and (Right) transmission mode, where the laser is opposite the transducer.

3. PHOTOACOUSTIC IMAGING < 200 MHZ

The high lateral resolution provided by OR-PAM is ideal for imaging single cells. High contrast photoacoustic images of specific cellular details can be targeted by using both the endogenous contrast in cells (e.g. hemoglobin) and exogenous contrast agents (e.g. dyes). Most studies use a custom-built PAM with transducers in the 20-60 MHz range, and pulsed lasers ranging from the UV to near-IR.

A. Imaging using Endogenous Chromophores

One of the primary advantages of PAM is the ability to perform label-free analysis of biological samples using endogenous chromophores, which include: hemoglobin in red blood cells (RBC), cytochromes in mitochondria, melanin in melanosomes, and DNA and RNA within the cell nucleus (figure 3.1). Hemoglobin is one of the most optically absorbing and abundant chromophores in the body throughout the visible spectrum, and provides excellent photoacoustic contrast in comparison to the weakly absorbing surrounding tissue. Many studies have exploited this fact to obtain high resolution images of single RBCs; one of the first applications of photoacoustic microscopy was imaging RBCs using OR-PAM with a 590 nm dye laser and a 75 MHz transducer [46]. The estimated resolution of the system was 5 μm, which was not sufficient to resolve fine details in a single 7.8 μm diameter RBC; however, this study showed that imaging single RBCs with near-optical resolution was possible. Using a 532 nm laser with a diffraction limited spot size, the resolution of the OR-PAM system was improved to 220 nm [47], which was sufficient to demonstrate the bi-concave shape of RBCs.

This article has been accepted for publication in a future issue of this journal, but has not been fully edited. Content may change prior to final publication. Citation information: DOI 10.1109/JSTQE.2015.2497323, IEEE Journal of Selected Topics in Quantum Electronics

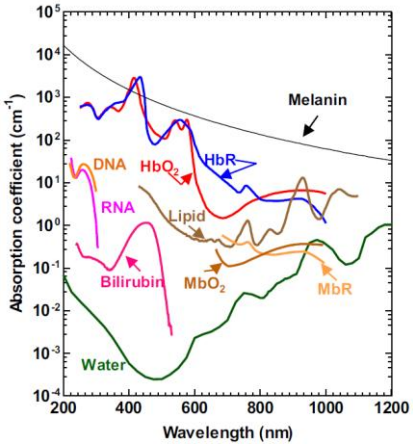

Figure 3.1: Optical absorption of endogenous chromophores commonly found in tissues. Figure reproduced from [44].

Tan et al. used PAM with a microcavity to image mildly and severely anemic RBCs [48]. Using a focused argon-ion laser, the photoacoustic signals from single blood cells were amplified by the microcavity and recorded using a microphone with 2.5 kHz bandwidth. Erythrocytes afflicted with anemia have reduced hemoglobin concentration of at the center of the cell, with a majority of the hemoglobin concentrated at the cell periphery. Due to this irregular hemoglobin distribution, photoacoustic images of these RBCs demonstrated dark central regions surrounded by rings of high photoacoustic signal that were observed to decrease in thickness with increasing anemia [49]. Using another microcavity equipped OR-PAM system with a 532 nm laser and a 50 MHz transducer, a resolution of 1 μm was achieved. While the resolution of this system was lower than other microcavity OR-PAM systems, the increased SNR provided by the amplification of the unique microcavity design enabled in-vivo imaging of blood vessels and single RBCs in a mouse ear [50].

Transient absorption ultrasonic microscopy (TAUM) was used to obtain photoacoustic images of RBCs with lateral and axial resolution in the micrometer range [51], [52]. This method used a laser pump pulse and probe pulse separated in time by a short delay. The pump and probe created separate photoacoustic emissions from the sample which were recorded by a 5 MHz ultrasound transducer. The photoacoustic signals overlapped temporally, but each signal could be extracted through frequency encoding of the excitation light. TAUM is a multi-photon process, which significantly improves the optical depth resolution in a way analogous to confocal microscopy [53]; thus, a high axial resolution can be achieved despite using a low frequency transducer which would typically have resolution in the hundreds of micrometers. However, this technique generally has poor SNR compared to other photoacoustic microscopy systems as the linear absorption is much stronger than the non-linear absorption, and it has limited utility in-vivo.

A technique called photoacoustic nanoscopy has been used to overcome the optical diffraction barrier and image single RBCs with a resolution of 88 nm using a 532 nm laser [54]. In this method, a laser pulse train with linearly increasing energy is focused onto the sample. The resulting photoacoustic amplitude increases non-linearly with each successive pulse due to optical saturation effects or nonlinear thermal expansion. The higher order non-linear absorption coefficient terms can be used to increase the resolution compared to the linear regime. With this technique, the lateral and axial resolutions improved past what was previously attainable using the tightly focused optical beam traditionally employed in OR-PAM. High resolution photoacoustic images of single RBCs were obtained with better detail than previous measurements (figure 3.2). However, precise control over the laser pulse parameters and energy measurements are necessary to achieve good SNR, which increases the hardware complexity and cost.

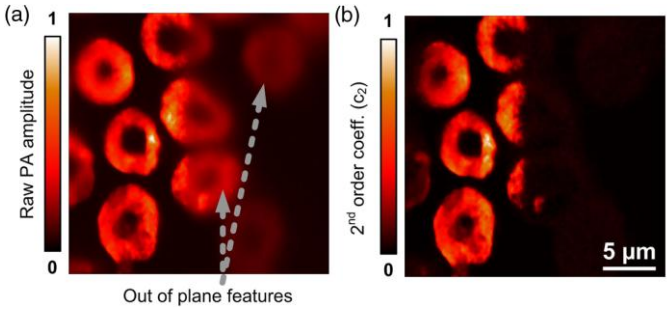

Figure 3.2: Photoacoustic images of single RBCs using conventional PAM (left) and photoacoustic nanoscopy (right). Lateral resolution below 100 nm and optical sectioning is possible using non-linear variations in the photoacoustic signal amplitude. Figure adapted from [54].

Recently, all optical detection methods have been developed for PAM [55]–[58]. Through the use of a micro-ring resonator and a 532 nm laser, Dong et al. developed a OR-PAM with a 0.7 μm lateral and 2.1 μm axial resolution [56]. The wide detection bandwidth (280 MHz) and excellent sensitivity enabled high resolution 3D reconstruction of a single RBC (figure 3.3), demonstrating its bi-concave shape in detail not observed previously [56]. A drawback to this technique that these systems require complex optical setups with narrow line-width lasers to achieve optimal performance. In addition to imaging single RBCs, OR-PAM has been used for creating high resolution 3D maps of vasculature in-vivo, however this topic is beyond the scope of this review; further details can be found in [37], [59]–[66].

This article has been accepted for publication in a future issue of this journal, but has not been fully edited. Content may change prior to final publication. Citation information: DOI 10.1109/JSTQE.2015.2497323, IEEE Journal of Selected Topics in Quantum Electronics

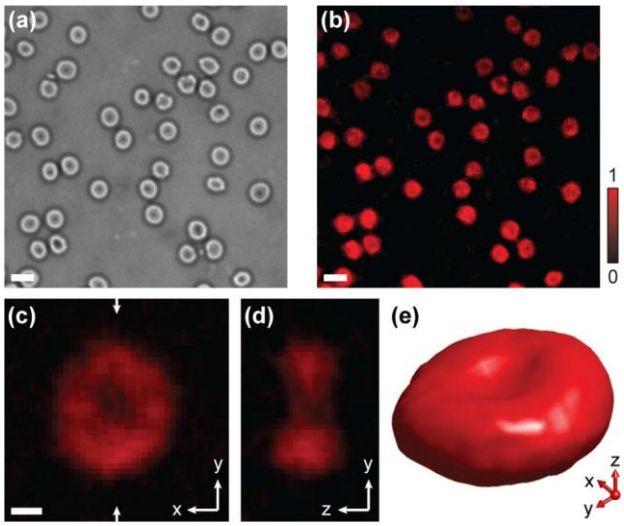

Figure 3.3: High resolution images of single RBCs using an all-optical photoacoustic method. Excellent lateral and axial resolutions are possible, enabling 3D reconstruction of a single RBCs in a mouse blood smear. (a) Optical image, (b) photoacoustic image, (scale bar 10 μm), (c) photoacoustic c-scan image of a RBC along the x–y plane (scale bar 2 μm), (d) cross-sectional image along the x–z plane, (e) 3D reconstruction of the RBC. Figure reproduced from [56].

Cytochromes, which are proteins that facilitate the production of energy in the mitochondria [67], have also been targeted as endogenous photoacoustic contrast agents. The cytochromes a, b, and c in the cell cytoplasm demonstrate absorbance at optical wavelengths around 420 nm, and have been used for imaging unstained fixed human fibroblasts [54], [68]. In this work, cytochromes within the fibroblast were targeted with an OPO laser tuned to 422 nm, and photoacoustic signals were recorded with a 40 MHz transducer. Acquired photoacoustic images were found to be consistent with fluorescence images of the same cells stained with MitoTracker Green FM (figure 3.4) [68]. In addition, by using nonlinear photoacoustic effects, super-resolution images of single mitochondria have been acquired using photoacoustic nanoscopy (figure 3.5) [54]. This technique was then used to image the mitochondrial network of fibroblast cells, and clearly demonstrated both the interconnected network in normal cells, and the expected fragmented network in Mitofusin knockdown cells [54].

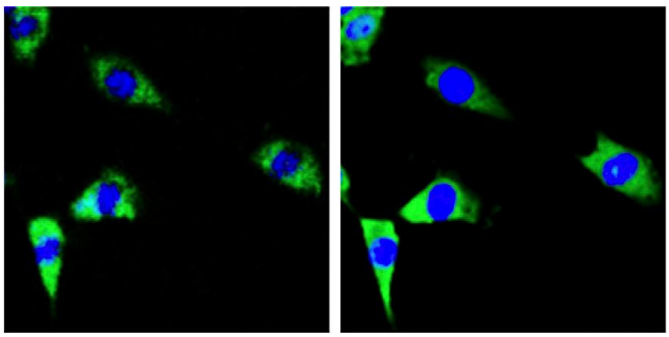

Figure 3.4: Photoacoustic (left) and optical fluorescence (right) images of fibroblasts. The photoacoustic image is a composite of images taken at 422 nm (green, absorption of cytochromes in the cytoplasm) and 250 nm (blue, absorption of DNA/RNA). The fluorescent images were stained to show the mitochondria in cytoplasm (MitoTracker green FM, green) and nucleus (4', 6-diamidino-2-phenylindole, blue). Figure reproduced from [68].

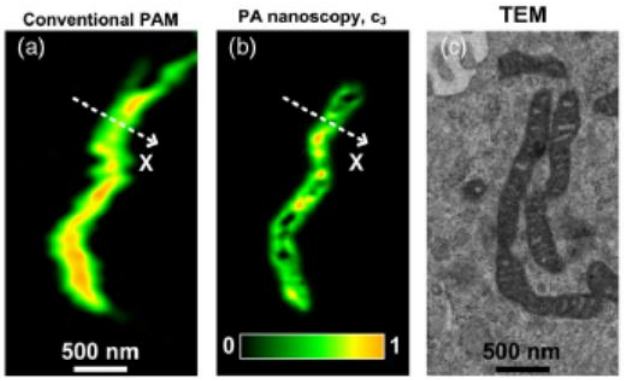

Figure 3.5: Photoacoustic images of single mitochondria using conventional PAM (left) and photoacoustic nanoscopy (middle), compared to a representative transmission electron microscope image (right). The resolution achieved using this method was 88 nm, several times better than what could be achieved using conventional PAM. Figure reproduced from [54].

The melanin pigment found in the melanosome organelle within melanocytes is another molecule which can be imaged with PAM. This pigment has been used to produce high resolution PAM images of melanocytes both in vivo and ex vivo. Using a fiber-based 1064 nm laser and a 40 MHz transducer, single melanoma cells on a glass slide were imaged with a 15 μm lateral resolution [69]. This resolution was sufficient to detect the shape of melanoma cells, but negligible detail within the cell was observed. Diffraction limited OR-PAM using a 532 nm laser and a 40 MHz transducer was used to create 220 nm resolution images of single fixed melanoma cells [47]. Strong photoacoustic signals from the cytoplasm were observed, with negligible signal from the nuclear area where melanin is uncommon (figure 3.6).

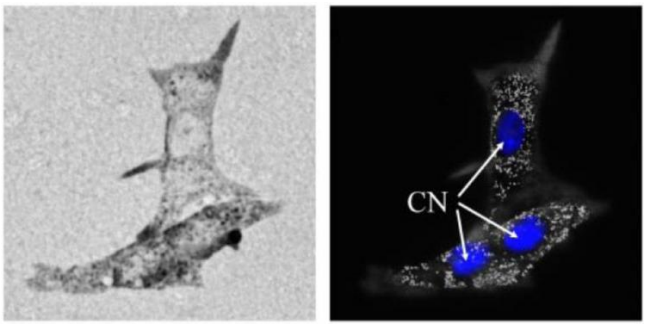

Figure 3.6: Optical (left) and photoacoustic (right) images of single melanoma cells. The stained cell nucleus (labeled CN) is marked for visibility in the photoacoustic image. Figure reproduced from [47].

A technique called photoimprint photoacoustic microscopy (PI-PAM) was used to achieve resolutions better than the optical diffraction limit [70]. This method used two successive photoacoustic images. In the first image, the photoacoustic signal from the entire laser focal spot is used to create a preliminary image of the sample. In the subsequent photoacoustic image, the chromophores within a laser spot were photobleached and thus contributed no signal; however

This article has been accepted for publication in a future issue of this journal, but has not been fully edited. Content may change prior to final publication. Citation information: DOI 10.1109/JSTQE.2015.2497323, IEEE Journal of Selected Topics in Quantum Electronics

the signals from any unbleached chromophores surrounding the laser spot still contributed to the image. The two images were subtracted, resulting in an image with resolution that was better that what could be obtained using conventional OR-PAM. This method was used to create photoacoustic images of melanoma cells with 90 nm lateral resolution [70]. Structural detail within the cell improved, particularly around the cell periphery. However, repeated imaging of the same region may not be possible due to the photobleaching of the chromophores. The photoacoustic nanoscopy technique was also used to create high resolution images of melanoma cells with 88 nm resolution [54]. This was sufficient to see melanin clusters within the cell that could not be seen with previous OR-PAM implementations.

DNA and RNA absorb strongly in the UV compared to the visible and near-IR spectrum [44], and can be targeted to provide high photoacoustic contrast images of cell nuclei. UV light at 250 nm was found to provide the highest contrast to noise images of cell nuclei in-vivo [71]. Combining this UV wavelength with a laser wavelength of 422 nm, the peak absorption for cytochrome, Yao *et al* demonstrated the feasibility of performing label-free photoacoustic imaging that provides information similar to that provided in histology. The photoacoustic histology images of fixed unstained human fibroblasts were similar to Hematoxylin and Eosin (H&E) stained samples [38], [68]. Using this method, ex vivo images of cell nuclei from mouse lip and intestinal epithelium, and in vivo images of nuclei in mouse ear skin were acquired [71], [72].

B. Imaging using Exogenous Chromophores

RBCs and melanocytes can generate high SNR photoacoustic images due to their strong optical absorption properties in the UV to near-IR spectrum. For other cells, an optically absorbing contrast agent is typically required to facilitate the generation of photoacoustic signals. This contrast agent is typically in the form of colorimetric stains, fluorescent dyes or nanoparticles [73], [74]. In histopathological assessment of biopsy samples, cells are stained to visualize cellular characteristics and tissue structure to identify diseases such as cancer [75]. However, if the counterstaining is weak, or if there is very little contrast between structures of interest, conventional optical microscopy techniques may be inadequate to view these variations. If biological stains with distinct optical absorption ranges are selected, a tunable laser may be used to target each individual stain, eliciting photoacoustic signals only from specific structures of interest.

Photoacoustic images can show enhanced detail of stained cells compared to their optical image counterparts. Zhang *et al.* used the Masson's trichrome to stain a sample of mouse connective tissue [76]. By using an OR-PAM with a laser tuned to wavelengths corresponding to the maximal absorption of the three colorimetric dyes incorporated in the stain, three PAM images were generated targeting the RBCs, cytoplasm, and collagen respectively. Superposition of the three images was shown to be in good agreement with optical images of the histology. The same group then imaged MC3T3 osteoblasts that had been stained with H&E. By tuning the wavelength of the laser to 523 nm, a photoacoustic image of both dyes was obtained. Subsequently tuning the laser to 587 nm produced an image with high signal originating from the Hematoxylin stained cell nuclei and negligible signal from the cytoplasm, enabling visual differentiation of the two structures (figure 3.7) [76]. The yellow tetrazolium dye MTT (3-(4,5-dimethylthiazol-2-yl)-2,5-diphenyltetrazolium bromide) is commonly used to assess viability of cells [77]. During metabolic activity, the terazolium dye is reduced to formazan, which has a purple color. This dye has been used as a photoacoustic contrast agent to image living fibroblasts, mouse embryonic stem cells, and breast cancer cells [78].

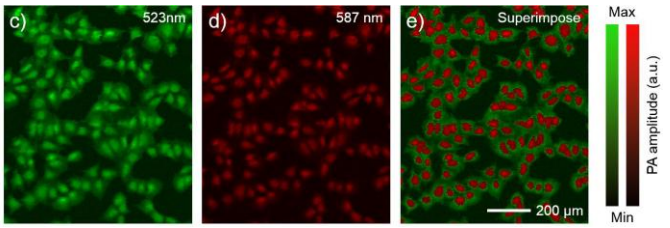

Figure 3.7: Photoacoustic images of MC3T3 osteoblast cells stained with H&E, imaged using (left) 532 nm, peak absorption of eosin Y, (middle) 587 nm, strong absorption from hematoxylin but not eosin, (right) composite image. Figure reproduced from [76].

Nanoparticles are ideally suited as contrast agents in photoacoustic imaging as their optical absorption can be up to 5 orders of magnitude greater than that of traditional molecular-based stains [79]. The absorption peak of gold nanoparticles can be tuned to the wavelength of the incident photons through the surface plasmon effect [80] to produce maximal photoacoustic signal. The nanoparticle surface can be modified to enhance biocompatibility, reduce toxicity, deliver a drug payload and enable targeting of specific cells or cell features [81]–[89]. These advantages have encouraged extensive use of nanoparticles as photoacoustic contrast agents for both in-vivo and ex-vivo applications [90]–[95], however this review will only concentrate on nanoparticles used in single cell imaging.

Gold nanocages have been used in conjunction with PAM to label and track mesenchymal stem cells both in vitro and in vivo [96]. Using an OR-PAM equipped with a 532 nm laser and a 40 MHz transducer, the stem cells were measured over 7 days. The photoacoustic signal intensity decreased over time as the cells divided and the number of nanocages per cell were diluted with each cell division. OR-PAM was used to image and quantify the uptake of nanoparticles by cells [97]. Using a 532 nm laser focused to a spot of 15 µm, murine macrophage cells were imaged after being incubated with spherical iron-oxide nanoparticles. A concentration of 1.1×10^5 nanoparticles/cell was estimated when cells were cultured in medium with a concentration of 3.7×10^{12} nanoparticles/mL. Using an OR-PAM equipped with a tunable pulsed laser and a 22 MHz transducer, the uptake of non-fluorescent gold nanorods into the cytoplasm of cultured MCF7 breast cancer cells has also been demonstrated(figure 3.8) [98]. The cells were incubated with gold nanorods that had a peak absorption of 720 nm. The cells were then fixed and stained with H&E. With 0.5 µm resolution, the cells were imaged first at 532 nm to create a photoacoustic image of the nucleus (from the H&E

stain), then again at 720 nm to create a photoacoustic image of the cytoplasm (from the gold nanorods).

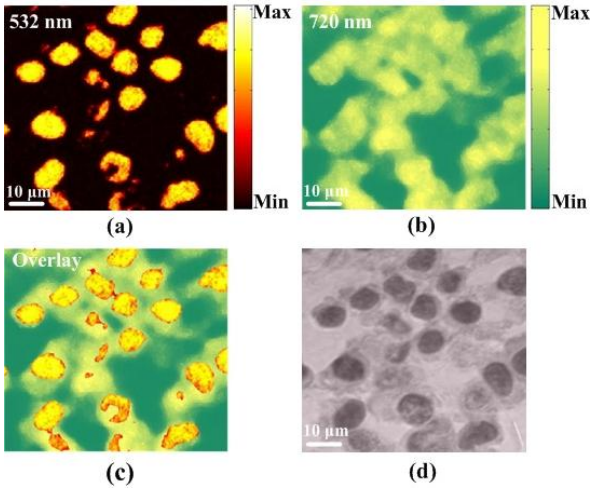

Figure 3.8: Photoacoustic images of MCF7 cells. (a) Photoacoustic image of MCF7 cell nuclei, (b) photoacoustic image of the cytoplasm containing gold nanorods, (c) composite of A and B, (d) optical image of the cells with H&E stain. Figure reproduced from [98].

4. Photoacoustic Imaging Using 1000 MHz

Photoacoustic imaging using ultra-high frequencies (UHF) over 100 MHz experienced a resurgence in the late 2000's with the availability of hardware capable of acquiring and analyzing high-frequency signals [99]–[103]. In addition to combined high resolution photoacoustic and ultrasound imaging, the wide-bandwidth (100's of MHz) of these UHF-PAM systems enables a quantitative analysis of the photoacoustic signal spectrum; however the transducers, electronics and hardware are more expensive than their lower frequency counterparts.

Currently, the only commercially available UHF photoacoustic microscope is made by Kibero GmbH (Saarbrucken, Germany). The system uses a transmission mode PAM setup with a 532 nm or 1064 nm pulsed laser, which is focused by the optics of an inverted optical microscope onto the sample. A transducer above the sample co-aligned with the optical axis records the laser-induced photoacoustic signals (figure 4.1). Further details on the system can be found in [104]–[106]. The UHF transducers in this system can also be used for pulse echo ultrasound measurements, enabling simultaneous acoustic and photoacoustic microscopy with micrometer resolution. As the focal spots of the ultrasound beam and laser spot are similar, UHF-PAM systems are a hybrid of both OR-PAM and AR-PAM, and thus demonstrate excellent lateral and axial resolutions. However, the short focal length of the transducers (50-100 μm) and high attenuation of the coupling medium at these frequencies typically limit sample analysis to single cells. Figure 4.2 shows the one-way acoustic attenuation as a function of depth and frequency through water at 25°C [107]. At 1000 MHz, a typical transducer focal length is 80 μm limiting measurements to a few cell monolayers at most, while a 10 MHz transducer can be used to measure signals through several centimeters of tissue [41].

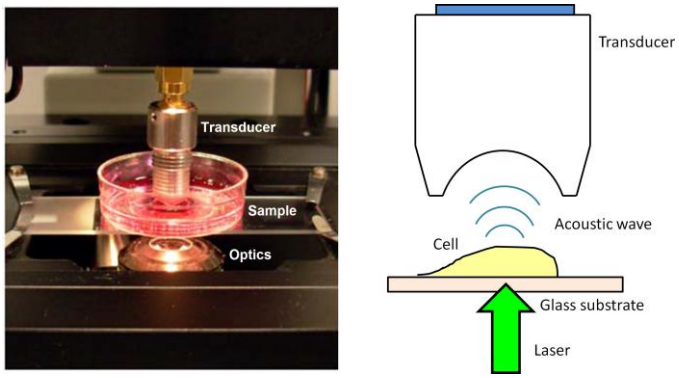

Figure 4.1 A photoacoustic microscope using UHF frequencies. (Left) the sample is positioned between the transducer and optics, (Right) A schematic showing irradiation of a single cell, and subsequent acoustic generation that is detected by the transducer 100 μm above the sample. Figure adapted from [108].

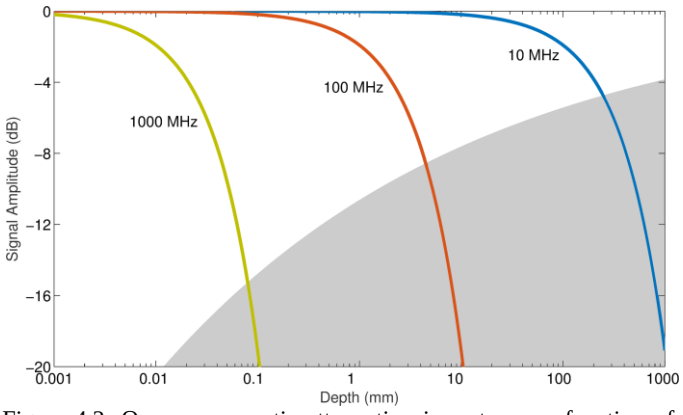

Figure 4.2: One-way acoustic attenuation in water as a function of frequency and depth for 10, 100 and 1000 MHz transducers. The shaded region indicates depths that are beyond the typical focal length of the transducer.

A. *Imaging using endogenous chromophores*

Hemoglobin and melanin absorb light from the UV into the near-IR (figure 3.1), and are ideally suited for photoacoustic imaging using the 532 nm laser in the UHF photoacoustic microscope. Figure 4.3 shows an optical and photoacoustic image of a single RBC on a glass substrate. The photoacoustic image was acquired using a 1200 MHz transducer and a 532 nm laser focused by a 10x optical objective with a 0.25 numerical aperture [106]. The contour of the RBC is clearly visible in the photoacoustic image due to the increased thickness of the cell at the periphery.

Figure 4.4 shows an optical and photoacoustic image of a B16-F1 mouse melanoma cell fixed on a glass substrate [106]. The optical image inset shows the nucleus stained for visibility. The photoacoustic image acquired using UHF-PAM at 1200 MHz clearly shows the inhomogenous melanin distribution throughout the cell cytoplasm. With a 1200 MHz transducer, the axial resolution of the UHF-PAM system is nearly 1 μm [106] which is sufficient to see topographical detail throughout the melanoma cell as demonstrated by the b-scan (cross-sectional view) shown in figure 4.4; the arrow in figure 4.3 indicates the location of the b-scan through the melanoma cell. The b-scan shows negligible signal within the

nuclear area; the signal is distributed around the sides and top of the cell where the melanin is located.

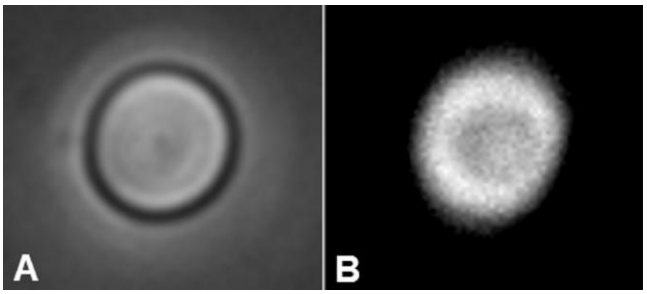

Figure 4.3: Optical (a) and photoacoustic (b) images of a single RBC measured at 1200 MHz. The contour of the bi-concave shape is visible in the photoacoustic image. The image size is 15x15 μm. Figure reproduced from [106].

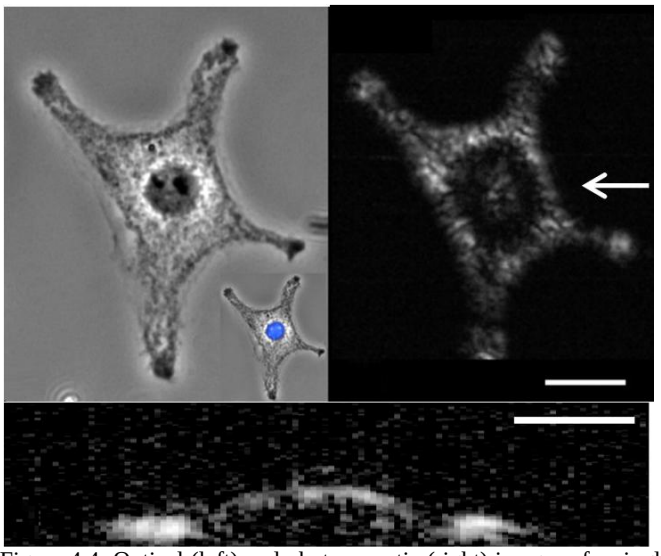

Figure 4.4: Optical (left) and photoacoustic (right) images of a single melanoma cell measured at 1200 MHz. The inset optical image shows the stained nucleus. The scale bar is 20 μm. (Bottom) B-scan cross-sectional photoacoustic image of the melanoma cell measured at the arrow. Figure reproduced from [106].

B. Imaging using exogenous chromophores

Colorimetric stains are commonly used to visually differentiate and identify cells in a sample. A common example is the Wright stain, which is applied to a blood smear to aid in visual identification of the different leukocytes present in a blood sample [109]. The Wright stain is typically composed of methylene blue, azure B and eosin Y, which are selectively absorbed by the different structures within each leukocyte type to give red, pink, blue and purple hues [110]. The range of colors, and hence, optical absorption properties, are ideal for photoacoustic imaging using multiple optical wavelengths.

Figure 4.5 shows optical and photoacoustic images of a neutrophil, lymphocyte and a monocyte acquired using an UHF photoacoustic microscope equipped with a 1000 MHz transducer and a fiber-coupled laser 532 nm laser [111]. The laser output from the fiber produced a wavelength continuum from 532 nm to about 610 nm via cascaded stimulated Raman scattering (SRS) [112]–[115], where the output wavelength was selected by using a 532 nm or a 600 nm filter.

The cell types could be identified according to the staining properties in the optical images. The photoacoustic images also enable identification of each cell type according to the unique optical absorption properties at both 532 and 600 nm. In the neutrophil, a strong photoacoustic signal was detected from the lobed nuclei at both wavelengths, with negligible signal in the cytoplasm. In the optical image of the lymphocyte, the nucleus was a deep purple color, with blue cytoplasm. In the corresponding photoacoustic images, the nucleus had a stronger photoacoustic signal than the cytoplasm at 532 nm, but this was reversed at 600 nm. The optical image of the monocyte showed the typical kidney-bean structure commonly observed in this cell type. The colors appear similar to the lymphocyte, however in the photoacoustic images, the nucleus produced the strongest photoacoustic signal at both 532 and 600 nm, despite having similar coloring to the lymphocyte. These three cell types could be easily differentiated according to the photoacoustic image amplitudes of the cytoplasm and nucleus.

In all cases, the photoacoustic signals from the leukocyte cytoplasm and nuclei were stronger than the surrounding RBCs. This illustrates the efficacy of stains in creating high amplitude photoacoustic signals from specific structures compared to endogenous absorbers. Additionally, several wavelengths can be used to create photoacoustic images based on the optical absorption properties of each cell, enabling identification of specific cells or features not visible using optical microscopy alone.

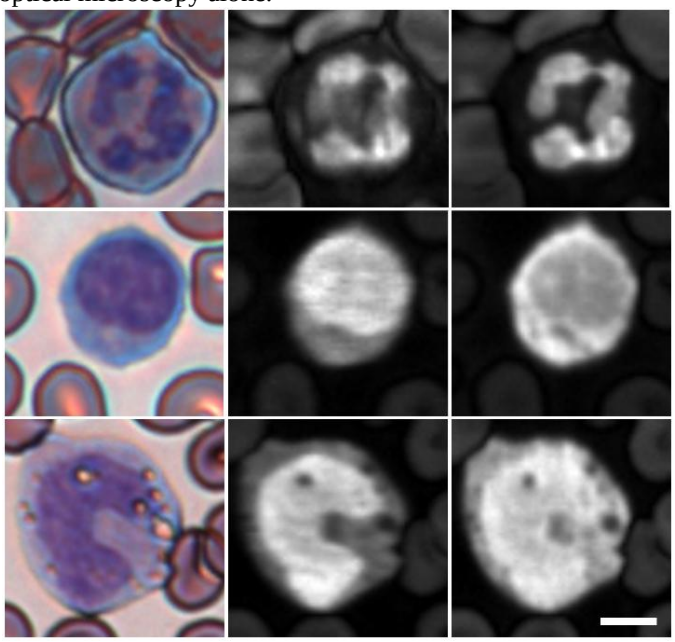

Figure 4.5: Optical and photoacoustic images of leukocytes from a blood smear, consisting of a neutrophil (top), a lymphocyte (middle) and a monocyte (bottom). The optical images (left) were stained with Wright-Giemsa, and the photoacoustic images were measured using a 1000 MHz transducer at laser wavelengths of 532 nm (middle) and 600 nm (right).The scale bar is 5 μm. Figure reproduced from [111].

This article has been accepted for publication in a future issue of this journal, but has not been fully edited. Content may change prior to final publication. Citation information: DOI 10.1109/JSTQE.2015.2497323, IEEE Journal of Selected Topics in Quantum Electronics

5. Quantitative Methods in Photoacoustics

A quantitative analysis of photoacoustic signals (QPA) enables both detection of individual cells and an extraction of cellular parameters. This includes functional properties such as the temperature and oxygenation status, and physical properties such as the size and shape. The size and mechanical properties of the cell affect the frequencies generated. The photoacoustic thermoelastic expansion model [22] was used to generate the photoacoustic signals as a function of frequency for a liquid sphere with diameter ranging from 100 nm to 100 µm with properties similar to those of a single cell (figure 5.1). The peak frequency and spectral features shift to higher frequencies as the object size decreases, which demonstrates the need for high frequency transducers for probing micrometer-sized objects such as single cells. A description of various quantitative methods are described in the next section.

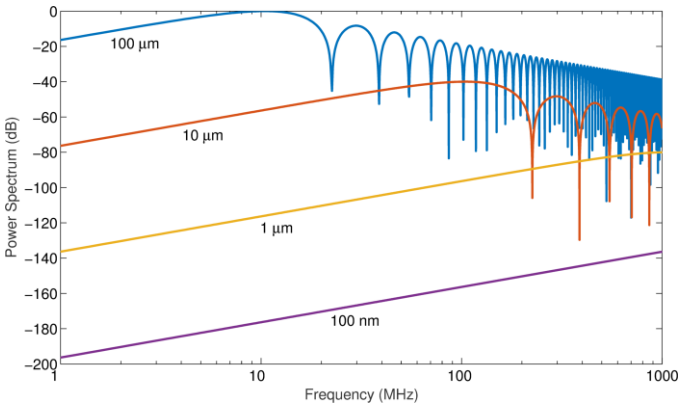

Figure 5.1: Photoacoustic spectra for a spherical cell with size ranging from 100 nm to 100 µm. The photoacoustic spectral maximum shifts to higher frequencies as the size decreases.

A. *Functional photoacoustics*

An analysis of functional parameters in-vivo can give insight into hemodynamic variations and biochemical processes that can help diagnose disease [13], [116]–[122]. Photoacoustic tomography is commonly used for examining functional parameters in-vivo, although options for functional analysis of single cells are limited due to acoustic attenuation and optical scattering through skin and tissues. There are, however, a few methods that can examine functional parameters at the single cell level both in-vivo and in-vitro.

Using a method called photoacoustic flowoxigraphy [123], the total hemoglobin concentration, oxygen saturation, oxygen saturation gradient, flow speed and oxygen release rate of single RBCs can be measured in-vivo via label-free photoacoustics. Using two lasers (532 and 560 nm) and a 50 MHz transducer, single RBCs flowing through a vessel in a mouse brain were measured. Figure 5.2 shows the system setup and the temporal changes in oxygenation in one of these RBCs as oxygen is released by the cell. The oxygen release rate increased as the oxygen saturation gradient and RBC flow rate increased. With excellent spatial and temporal resolution, photoacoustic flowoxigraphy has clinical applications in monitoring cancer therapy, probing tissue microenvironments and response to stimuli and functional imaging.

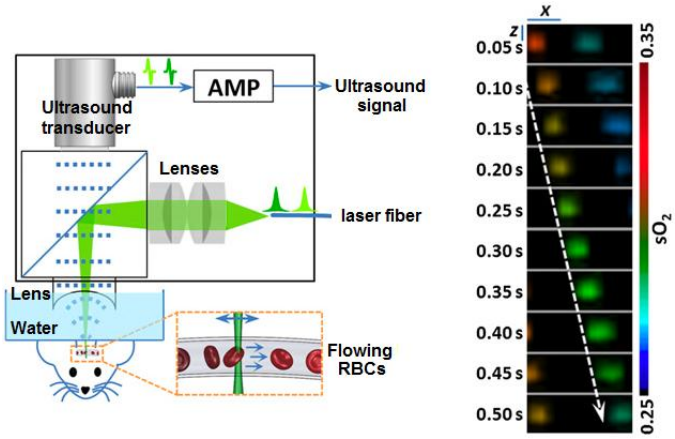

Figure 5.2: Oxygen saturation of a single RBC flowing in-vivo. (Left) The schematic showing the photoacoustic microscope, (Right) The oxygen saturation (sO_2) decreases as oxygen is released into the surroundings. Figure reproduced from [123].

The intracellular temperature can be measured using changes in the amplitude of photoacoustic signals emitted from single cells. Using a photoacoustic microscope equipped with a 532 nm pulsed laser and a 75 MHz transducer, cells incubated with iron oxide microparticles were imaged while the temperature of the surrounding media was gradually increased using a heating pad [124]. The average photoacoustic signal amplitude of a single cell increased by nearly 25% when heated from 26 to 34 degrees over a 10 minute period. The local temperature is related to the temperature dependent Grüneisen parameter, and allows for the calculation of the intracellular temperature. Figure 5.3 shows the photoacoustic derived change in temperature throughout a single cell when heated by a few degrees over 400 seconds using this method. Fluorescence assisted photoacoustic thermometry (FAPT) is another method that may be used to determine the intracellular temperature [125]. If the ratio of fluorescence intensity to photoacoustic amplitude of a fluorophore at a given temperature is known, the local temperature at each point in the cell can be mapped through simultaneous photoacoustic and fluorescence measurements. Using this technique, the mitochondria in HeLa cells were stained with Mitotracker Orange and were subsequently probed using a photoacoustic microscope with a 532 nm pulsed laser and a 40 MHz transducer. The temperature map of the stained HeLa cells is shown in figure 5.3, along with the optical image and the fluorescence image of Mitotracker Orange.

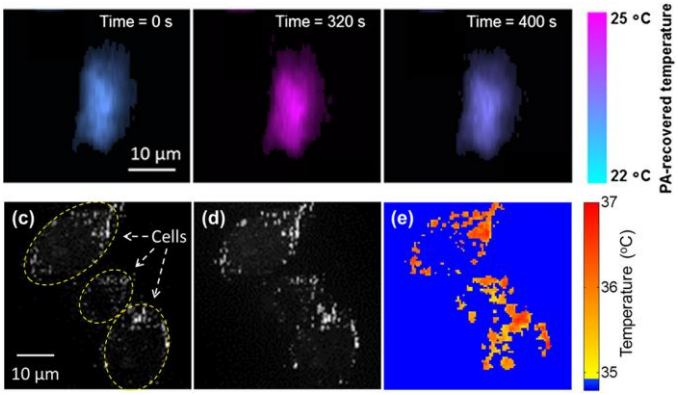

Figure 5.3: (Top) Photoacoustic thermometry of a single cell containing iron oxide microparticles during heating at different times. (Bottom) Photoacoustic (left) and temperature mapped (right) images of single Hela cells stained with Mitotracker Orange. Figures adapted from [124], [125].

B. Photoacoustic detection of flowing cells

Photoacoustic-based Doppler measurements can be used to determine the flow rate of blood in-vivo. The systems do not have the resolution to detect single cells, and so use superposition of signals within an interrogated volume to detect specific cells that absorb at the interrogating wavelength. Most studies utilizing flow systems are designed to detect melanoma cells due to their high natural optical absorption properties, however other cells have been detected using contrast agents such as magnetic and gold nanoparticles.

Zharov and colleagues pioneered an in-vivo method to detect cells flowing in blood vessels using photoacoustic flow cytometry (PAFC). A high repetition rate laser is directed through the skin, and an ultrasound transducer records the resulting photoacoustic signals. This method has been used to determine cell flow rates [126], and to detect leukocytes, circulating tumor cells, nanoparticles and bacteria flowing in the bloodstream and cerebrospinal fluid, as well as nanoparticle labeled cancer cells in the lymph [127]–[132]. Fluorescence detection and photothermal measurements can further be combined with photoacoustics to increase the specificity of the technique [131], [132]. They discovered that nanoparticles, dyes and melanoma cells have ultrasharp nonlinear resonances when using laser energies sufficient to create localized nano- and microbubbles [133]. This can be used to increase photothermal and photoacoustic detection specificity, particularly with the PAFC technique. Using the PAFC system, they have shown that cancer cells are released into the bloodstream during interventions such as surgery or biopsy of a tumor (figure 5.4) [134]–[136]. There are many applications for an in-vivo photoacoustic detection system, ranging from diagnostic screening for cancer and other diseases to evaluating prognosis and treatment efficacy during cancer therapy. Comprehensive reviews cover aspects of this new technology in more detail are provided in [134]–[138].

A combined photoacoustic and ultrasound system to identify and capture tumor cells using magneto-optical coupled nanoprobes was developed by Hu *et al* [139]. Silica-coated gold nanoparticles containing iron oxide and folic acid on the shell were used to tag HeLa cells which flowed through the detection system. Magnets trapped only the tagged HeLa cells, which were then detected using a tunable pulsed laser and a linear array ultrasound transducer (figure 5.5). Over time, the photoacoustic signal from the target area increased as the number of captured cells increased. This high throughput system can detect and trap cells at the single cell/mL range, and has potential for high sensitivity detection of circulating tumor cells.

Viator and colleagues developed a photoacoustic method to detect circulating melanoma cells in blood samples in-vitro. Using a microfluidic device, the sample flow is split into microsized “slugs” which are probed using a 532 nm pulsed laser and a 45 MHz transducer [140], [141]. A slug containing a melanoma cell generates a higher amplitude photoacoustic signal than a slug containing just blood cells, and thus the presence of melanoma cells in a sample can be detected. This system can also capture the slugs containing melanoma cells for further examination.

A photoacoustic method for detecting flowing melanoma cells in-vitro using a 1064 nm pulsed fiber-laser was demonstrated by Wang and colleagues [69]. Melanoma cells were suspended in bovine blood and flowed through a glass microtube, while a laser was scanned through a cross sectional area creating b-scans. The photoacoustic amplitude from the melanoma cells was four times larger than the blood background, enabling identification and counting of flowing melanoma cells. The 50 kHz laser repetition rate combined with a laser-scanning microscope enabled a scanning frame rate in the kHz range [142]. Instead of scanning the laser across the microtube, the laser spot could be fixed in place to create m-mode images of flowing melanoma cells [143] which can be used to size cells if the flow speed is known.

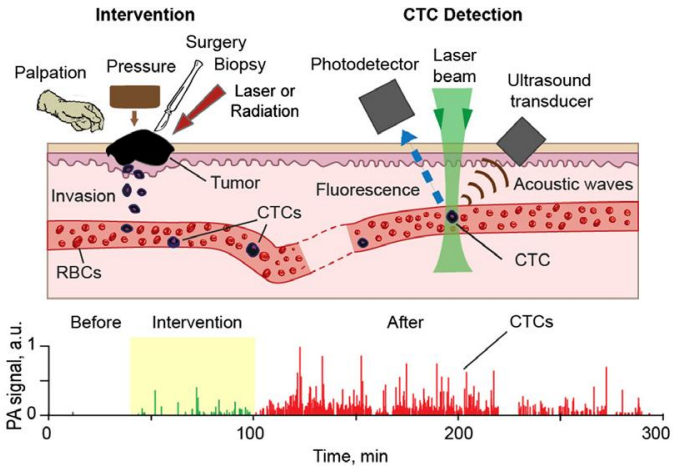

Figure 5.4: (Top) Schematic showing how CTCs are detected using photoacoustic flow cytometry in-vivo after an intervention (Bottom) The number of CTC events detected before, during and after the intervention. Figure reproduced from [136], [137].

This article has been accepted for publication in a future issue of this journal, but has not been fully edited. Content may change prior to final publication. Citation information: DOI 10.1109/JSTQE.2015.2497323, IEEE Journal of Selected Topics in Quantum Electronics

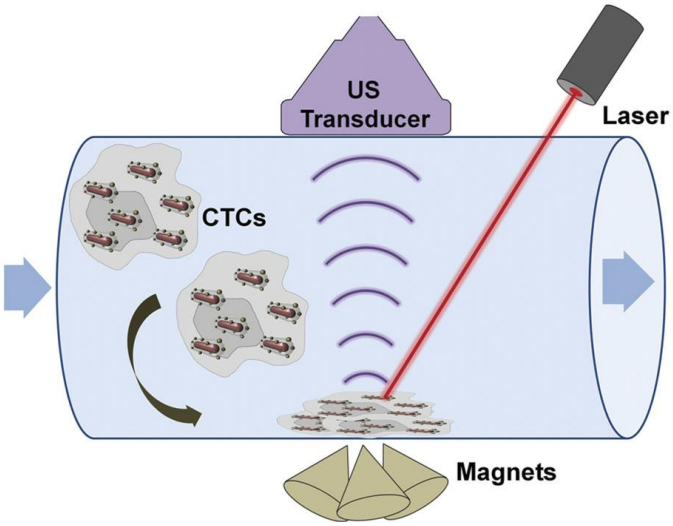

Figure 5.5: Detection and trapping of CTCs labeled with magnetic nanoparticles ex-vivo. The photoacoustic signal is related to the number of CTCs trapped at the magnet. Figure reproduced from [139].

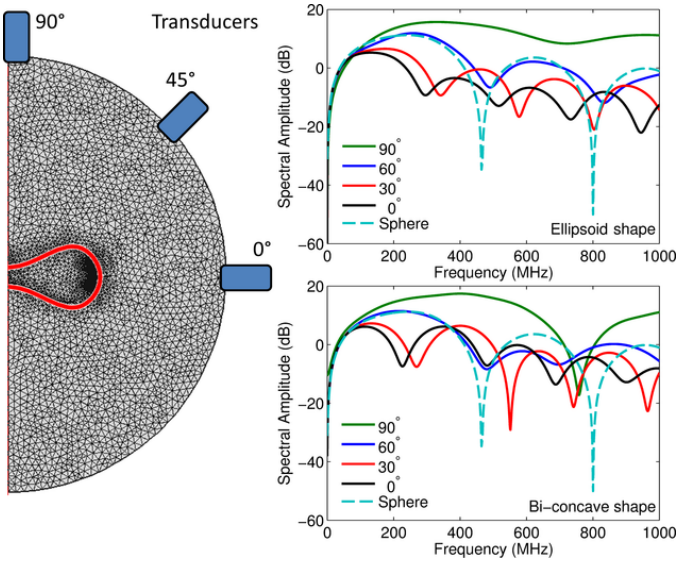

Figure 5.6: The photoacoustic FEM design showing the RBC at the middle (left), and the FEM simulation results for a RBC with a ellipsoid shape (top), bi-concave shape (bottom) and spherical shape (dashed line on both plots) at measured angles of 0, 30, 60 and 90 degrees relative to the RBC. Figure adapted from [147].

C. Red blood cells

Numerous photoacoustic-based methods can detect RBCs, but have difficulty determining their size, morphology or other biomechanical properties. Optical and electrical based measurement systems and hematology analyzers typically approximate their shape as spheres for simplicity [144]. Analytical solutions for the photoacoustic signals emitted by single bi-concave RBCs do not exist; however, finite element models (FEMs), which are commonly used to solve complex geometries, have been used to generate these responses and validate UHF signal measurements [145], [146].

To model the photoacoustic signals generated by red blood cells, a transient acoustics 2D axi-symmetric model was developed to simulate the photoacoustic pressure wave generated from single RBCs that uniformly and instantaneously absorb optical energy (figure 5.6) [147], [148]. The photoacoustic signals of bi-concave, ellipsoid and spherical RBCs with constant volume if 94 μm^3 were investigated at angles of 0, 30, 60 and 90° (relative to the transducer axis) around the RBC. Figure 5.6 hows the photoacoustic signal power spectrum from a spheroid-shaped and bi-concave shaped RBC, respectively; a spherical RBC is shown for reference. Each solid curve denotes the angle relative to the transducer. From frequencies 0-100 MHz, there is significant overlap in the spectral shape between the ellipsoid and bi-concave shape, demonstrating the insensitivity to cell morphology within this frequency range. As the frequency increases, differences in the spectral shape occur for both the cell shape and orientation, and it becomes apparent that the bi-concave shape is required to obtain accurate simulation results. These simulations demonstrate the necessity of UHF transducers with frequencies in the 100-500 MHz range for performing QPA on single RBCs.

The photoacoustic signals from single RBCs in a vertical and horizontal orientation were measured and compared to the FEM simulations. A 532 nm pulsed laser and a transducer with a 375 MHz center frequency and bandwidth of 250 MHz were used to measure signals from a single RBC in vertical and horizontal orientations as shown in figure 5.7. The time domain signal of the horizontally oriented RBC is much greater than the vertically oriented RBC, however the power spectrum shows more specific features that can be used to easily differentiate the two RBC orientations. The spectrum of the horizontal RBC is nearly flat over the bandwidth of the transducer, while the vertical RBC shows two spectral minima at 210 and 550 MHz. The theoretical spectra for the two orientations calculated using the previously described FEM is shown as a dotted line, and is in good agreement with both measurements [147].

To probe photoacoustic spectral features at higher frequencies, a transducer with a 1200 MHz center frequency was used to measure the signals from horizontally oriented RBCs [106]. The time domain signal from a single RBC, and the power spectra from four RBCs measured using the 1200 MHz transducer and a 532 nm pulsed laser are shown in figure 5.8. In the power spectra, two minima are observed at around 825 MHz and 1500 MHz. The first minima agrees well with the theoretical predictions for a horizontal RBC shown in figure 5.7. The wide bandwidth (670 MHz) of the transducer enables an analysis of a very wide frequency range, however the difficulties with SNR and low depth of field (< 10 μm) make these UHF measurements considerably more difficult to perform than those at lower frequencies.

This article has been accepted for publication in a future issue of this journal, but has not been fully edited. Content may change prior to final publication. Citation information: DOI 10.1109/JSTQE.2015.2497323, IEEE Journal of Selected Topics in Quantum Electronics

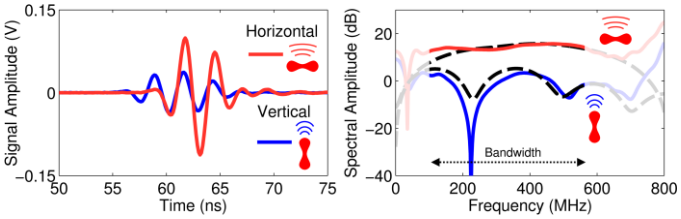

Figure 5.7: The time domain signal (left) and photoacoustic power spectrum (right) of a single RBC measured at 375 MHz in a vertical (blue) and horizontal (red) orientation relative to the transducer. The dashed line shows the theoretical predictions using FEM simulations. Areas outside the transducer bandwidth have been shaded. Figure reproduced from [147].

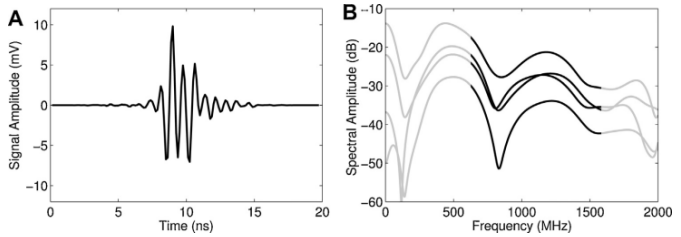

Figure 5.8: The measured time domain signal (left) and photoacoustic power spectra (right) of four RBCs measured at 1200 MHz. Areas outside the transducer bandwidth have been shaded. Figure reproduced from [106].

The theoretical modeling and experimental measurements show that the photoacoustic spectrum over 100 MHz is highly sensitive to the orientation and morphology of cells. Provided the laser pulse width is short enough to ensure a broadband signal with high frequency content, this sensitivity can be used to examine how the shape of a RBC changes due to external conditions, with applications towards diagnosing blood-related diseases such as sickle cell anemia. The sensitivity of photoacoustic waves to changes in RBC morphology was examined by measuring RBCs in phosphate buffered saline (PBS) with varying osmolalities ranging from isotonic (294 mmol/kg, which maintains the normal bi-concave shape) to hypotonic (90 mmol/kg, which induces a spherical RBC shape) [147]. The photoacoustic signals of 21 RBCs were measured at different osmolalities using a 532 nm laser and a 375 MHz transducer as shown in figure 5.9. The error bars indicate the standard deviation. As the osmolality was decreased to hypotonic conditions, the shape of the power spectrum changed with a shift to lower frequencies. A quantitative analysis of the power spectra shows that the photoacoustic power spectral amplitude (at 288 MHz) and spectral slope (from 275-300 MHz) can be used to differentiate changes in RBC morphology from 294 to 118 mmol/kg with high confidence as shown in table 4.1 ($p<0.001$). No difference was observed between 118 and 94 mmol/kg; the RBC shape was spherical at both osmolalities, and thus the spectra should be similar.

The sensitivity of the photoacoustic spectral measurements to identify artificially induced echinocyte morphologies was then examined [147]. Photoacoustic signals from 21 healthy RBCs in a horizontal orientation were measured in DMEM. The RBCs were added to PBS and left at 4°C for 24 hours, a process which depletes the ATP reserves within the RBCs and causes echinocytes to form. The photoacoustic signals from the echinocytes were measured, then the RBCs were immediately immersed in DMEM to restore the normal bi-concave shape before subsequent photoacoustic signals were acquired. Figure 5.9 shows these results along with representative optical images. The photoacoustic spectra of the fresh RBCs (black curve) and restored RBCs (red curve) nearly overlap, while the ATP-depleted RBCs (blue curve) is 20 dB lower than the other cells. These measurements show that the irregularly shaped echinocytes can be differentiated from normal healthy RBCs based solely on their photoacoustic power spectrum, and also that echinocytes can completely regain their normal bi-concave shape in certain conditions. These procedures can be applied to examine how photoacoustic signals can be used to identify RBC-related diseases and infection that alter the morphology, including spherocytosis, anemia, and malaria.

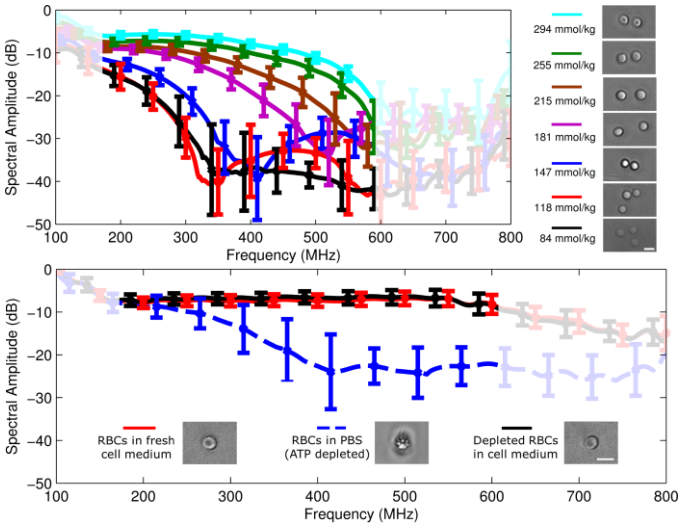

Figure 5.9: (Top) The photoacoustic spectra of 21 RBCs measured at osmolalities ranging from isotonic (294 mmol/kg) to hypotonic (84 mmol/kg). (Bottom) Photoacoustic spectra of 21 healthy RBCs measured in cell medium (red), 21 echinocytes (blue), then the echinocytes immersed in cell medium to restore their healthy status (black). Areas outside the transducer bandwidth have been shaded. Figure reproduced from [147].

Osmolality (mmol/kg)	Spectral amplitude at 288 MHz (dB)	Spectral slope at 275-300 MHz (dB/MHz)
294	-5.8 ± 0.7	-0.006 ± 0.004
255	-7.4 ± 0.9	-0.009 ± 0.004
215	-9.3 ± 1.1	-0.022 ± 0.006
181	-11.0 ± 1.1	-0.042 ± 0.012
147	-18.1 ± 2.3	-0.112 ± 0.026
118	-26.1 ± 3.7	-0.217 ± 0.073
84	-25.2 ± 5.4	-0.176 ± 0.084

Table 5.1: The spectral amplitude, and spectral slope of 21 RBCs measured at different osmolalities [147].

D. Single cell characterization

Ultrasound and photoacoustic measurements are highly compatible due to similar hardware requirements and analysis methods. By adding a laser and integrated trigger, many

This article has been accepted for publication in a future issue of this journal, but has not been fully edited. Content may change prior to final publication. Citation information: DOI 10.1109/JSTQE.2015.2497323, IEEE Journal of Selected Topics in Quantum Electronics

ultrasound systems can be converted for dual modality measurements using ultrasound and photoacoustics [149]–[154], however these systems are limited by the sensing frequency of the transducer. Typically ultrasound and photoacoustic frequencies over 100 MHz are required to extract information about single cells that can be used to identify them and determine their size.

Healthy blood contains RBCs and leukocytes, as well as platelets and other biochemicals. People with cancer may also have circulating tumor cells present [155]–[157]. Detection of melanoma cells is particularly attractive for photoacoustic measurements due to their natural endogenous optical absorption properties and opportunities for label-free photoacoustic detection. Leukocytes are 7-12 μm in diameter, while melanoma cells are typically larger at 15-20 μm in diameter. The ability of ultrasound and photoacoustic measurements to differentiate and determine the size of human leukocytes and circulating B16-F1 mouse melanoma cells in-vitro were examined using a UHF photoacoustic microscope [108]. Typical photoacoustic and ultrasound signals and power spectra recorded from a melanoma cell and a leukocyte are shown in figure 5.10. Both an ultrasound and photoacoustic signal were measured from the melanoma cells, while only ultrasound signals were measured from the leukocytes due to the lack of a prominent endogenous chromophore at 532 nm.

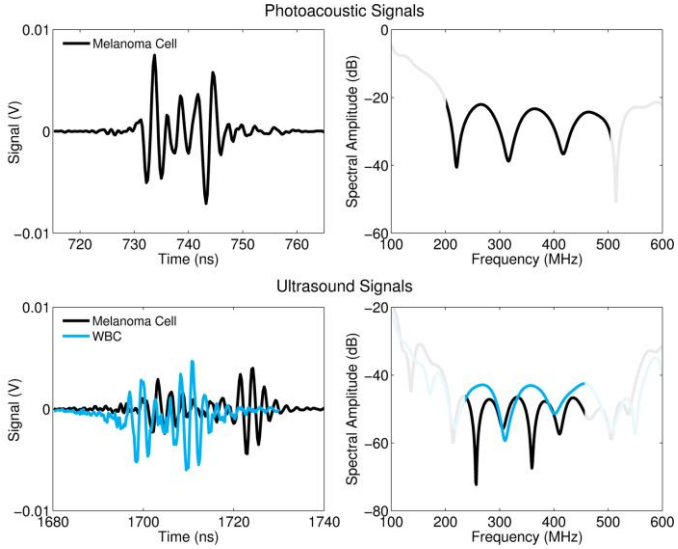

Figure 5.10: The photoacoustic (top) and ultrasound (bottom) time domain signal (left) and power spectra (right) of a melanoma cell and WBC measured using 375 MHz. Areas outside the transducer bandwidth have been shaded. Figure reproduced from [108].

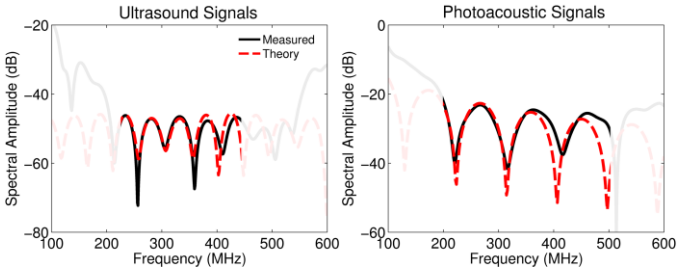

Figure 5.11: The ultrasound power spectra (left) and photoacoustic power spectra (right) of a single melanoma cell compared to theoretical predictions. Areas outside the transducer bandwidth have been shaded. Figure reproduced from [108].

Cell Type	Number measured	Ultrasound Spectral Spacing (MHz)	Calculated cell size
WBC (small)	23	102 ± 9	8.0 ± 0.7
WBC (large)	5	73 ± 8	11.3 ± 1.3
Melanoma (ultrasound)	47	51 ± 15	17.1 ± 4.4
Melanoma (photoacoustic)	47	99 ± 23	17.0 ± 4.6

Table 5.2: The average cell size of WBCs and melanoma cells estimated from the ultrasound and photoacoustic power spectra [108].

Cells in suspension have a spherical shape. Under the assumption that the cell is homogeneous on the probing length scales used and that it uniformly and instantaneously absorbs the laser energy, they can be modeled using a spherical photoacoustic analytical model [23]. Analytical solutions for the ultrasound scattering from liquid spheres is well established, dating back to 1950 [158]–[162]. The cell size can be calculated by comparing the frequency location of the spectral minima to theoretical predictions. Figure 5.11 shows the measured ultrasound and photoacoustic spectra from a single melanoma cell, along with the theoretical solution best fit from ultrasound and photoacoustic theory. The calculated diameter was 16.9 μm using ultrasound, and 17.2 μm using photoacoustics, in line with expected values.

This procedure was performed for 28 leukocytes and 47 melanoma cells to determine the size distribution using ultrasound and photoacoustics (table 4.2). For the leukocytes, it was found that the size distribution was bimodal, where 23 cells had an average size of 8.0 ± 0.7 μm, and another 5 cells had an average size of 11.3 ± 1.3 μm. This fits in well with the expected size of live leukocytes measured using flow cytometery and a coulter counter, where the mean diameter of cells was 7 μm (for lymphocytes), 8.4 μm for neutrophils and nearly 9 μm for monocytes [163]. The average diameter of 47 melanoma cells using ultrasound measurements was 17.1 ± 4.4 μm, and 17.0±4.6 μm using photoacoustics. The ultrasound and photoacoustic method of determining the cell size was the similar within error ($p<0.001$), despite different physical mechanisms of generating the sound waves. These results show that ultrasound and photoacoustics can be used to count and size cells, and identify the cell type according to the spectral patterns and amplitude [108]. The manual measurement process in the acoustic microscope is time consuming; fewer than 100 cells can be measured during a typical experiment. However these measurements could be adapted to a flow system [164], in which cells flow by a target area where they are insonified with an ultrasound beam and irradiated with a pulsed laser. In this system, thousands of cells could be measured per second, sufficient to provide a statistical analysis of the cell properties. Such a system could eventually be used to help diagnose disease due to variations in the cell size, shape and structure.

6. Concluding Remarks

PAM of single cells has experienced significant growth within the past decade. Advances in laser technology, ultrasound and electronics hardware, and signal processing techniques have improved imaging resolution from 5-10 μm in the early 2000's, to less than 100 nm today. High resolution images with sub-cellular detail can be created by targeting either endogenous chromophores such as hemoglobin and melanin, or exogenous contrast agents such as nanoparticles and dyes. Technology advances have also given rise to novel quantitative analysis techniques which offer insight into functional information, and can be used to infer structural or biomechanical properties at the single cell level. Despite these advances, PAM has largely remained a research tool. Clinical applications of single cell PAM remain in their infancy, and further work is required to translate this technology for clinical use. The technology is rapidly advancing, and it is only a matter of time before more applications emerge and PAM sees routine use in the clinic.

7. Acknowledgements

This research was undertaken, in part, thanks to funding from a Canadian Cancer Society Innovation Grant generously supported by the Lotte & John Hecht Memorial Foundation (grant #702161), the Natural Sciences and Engineering Research Council of Canada, and the Canada Research Chairs Program. Funding to purchase the equipment was provided by the Canada Foundation for Innovation, the Ontario Ministry of Research and Innovation, and Ryerson University.

References

[1] A. Bell, "On the Production and Reproduction of Sound by Light," *American Journal of Sciences*, vol. XX, no. 118, pp. 305–324, Oct. 1880.

[2] A. G. Bell, "The production of sound by radiant energy," *Science*, vol. os-2, no. 49, pp. 242–253, May 1881.

[3] J. Tyndall, "Action of an intermittent beam of radiant heat upon gaseous matter," *Journal of the Franklin Institute*, vol. 111, no. 4, pp. 297–308, Apr. 1881.

[4] W. C. Röntgen, "On tones produced by the intermittent irradiation of a gas," *Philosophical Magazine Series 5*, vol. 11, no. 68, pp. 308–311, Apr. 1881.

[5] A. Rosencwaig, "Photoacoustic spectroscopy," *Advances in electronics and electron physics*, vol. 46, pp. 207–311, 1978.

[6] A. Rosencwaig, "Photoacoustic spectroscopy of solids," *Optics Communications*, vol. 7, no. 4, pp. 305–308, Apr. 1973.

[7] A. Rosencwaig and A. Gersho, "Theory of the photoacoustic effect with solids," *Journal of Applied Physics*, vol. 47, no. 1, pp. 64–69, Jan. 1976.

[8] A. Rosencwaig, "Photoacoustic Spectroscopy of Biological Materials," *Science*, vol. 181, no. 4100, pp. 657–658, Aug. 1973.

[9] P. M. Morse and K. U. Ingard, *Theoretical Acoustics*. McGraw-Hill Inc.,US, 1968.

[10] V. Z. Gusev and A. A. Karabutov, *Laser Optoacoustics*. New York: American Institute of Physics, 1992.

[11] L. V. Wang, "Tutorial on Photoacoustic Microscopy and Computed Tomography," *IEEE Journal of Selected Topics in Quantum Electronics*, vol. 14, no. 1, pp. 171 –179, Feb. 2008.

[12] H. K. Wickramasinghe, R. C. Bray, V. Jipson, C. F. Quate, and J. R. Salcedo, "Photoacoustics on a microscopic scale," *Applied Physics Letters*, vol. 33, no. 11, pp. 923–925, Dec. 1978.

[13] P. Beard, "Biomedical photoacoustic imaging," *Interface Focus*, vol. 1, no. 4, pp. 602–631, Aug. 2011.

[14] M. Xu and L. V. Wang, "Photoacoustic imaging in biomedicine," *Review of Scientific Instruments*, vol. 77, no. 4, pp. 041101–041101–22, Apr. 2006.

[15] F. A. McDonald, "Photoacoustic effect and the physics of waves," *American Journal of Physics*, vol. 48, no. 1, pp. 41–47, Jan. 1980.

[16] F. A. McDonald, "Practical quantitative theory of photoacoustic pulse generation," *Applied Physics Letters*, vol. 54, no. 16, pp. 1504–1506, Apr. 1989.

[17] C. G. a. Hoelen and F. F. M. de Mul, "A new theoretical approach to photoacoustic signal generation," *The Journal of the Acoustical Society of America*, vol. 106, no. 2, p. 695, 1999.

[18] L. V. Wang, *Photoacoustic Imaging and Spectroscopy*. CRC Press, 2009.

[19] G. Paltauf and P. Dyer, "Photomechanical processes and effects in ablation," *Chemical Reviews*, vol. 103, no. 2, pp. 487–518, 2003.

[20] G. J. Diebold, M. I. Khan, and S. M. Park, "Photoacoustic 'Signatures' of Particulate Matter: Optical Production of Acoustic Monopole Radiation," *Science*, vol. 250, no. 4977, pp. 101–104, Oct. 1990.

[21] L. V. Wang and H. Wu, *Biomedical Optics: Principles and Imaging*, 1 edition. Hoboken, N.J: Wiley-Interscience, 2007.

[22] G. Diebold, "Photoacoustic monopole radiation: waves from objects with symmetry in one, two and three dimensions," in *Photo-acoustic Imaging and Spectroscopy*, L. Wang, Ed. Taylor and Francis, 2009, pp. 3–17.

[23] G. Diebold and P. Westervelt, "The photoacoustic effect generated by a spherical droplet in a fluid," *The Journal of the Acoustical Society of America*, vol. 84, p. 2245, 1988.

[24] G. J. Diebold, T. Sun, and M. I. Khan, "Photoacoustic monopole radiation in one, two, and three dimensions," *Physical Review Letters*, vol. 67, no. 24, pp. 3384–3387, 1991.

[25] M. Khan, T. Sun, and G. Diebold, "Photoacoustic waves generated by absorption of laser radiation in optically thin cylinders," *The Journal of the Acoustical Society of America*, vol. 94, no. 2, p. 931, 1993.

[26] J. Zalev and M. C. Kolios, "Exact solution for a photoacoustic wave from a finite-length cylindrical source," *The Journal of the Acoustical Society of America*, vol. 137, no. 4, pp. 1675–1682, Apr. 2015.

[27] Y. Li, H. Fang, C. Min, and X. Yuan, "Analytic theory of photoacoustic wave generation from a spheroidal droplet," *Optics Express*, vol. 22, no. 17, p. 19953, Aug. 2014.

[28] R. Lemons and C. Quate, "Acoustic microscopy: biomedical applications," *Science*, vol. 188, no. 4191, pp. 905 –911, May 1975.

[29] R. L. Thomas, J. J. Pouch, Y. H. Wong, L. D. Favro, P. K. Kuo, and A. Rosencwaig, "Subsurface flaw detection in metals by photoacoustic microscopy," *Journal of Applied Physics*, vol. 51, no. 2, p. 1152, 1980.

[30] J. J. Pouch, R. L. Thomas, Y. H. Wong, J. Schuldies, and J. Srinivasan, "Scanning photoacoustic microscopy for nondestructive evaluation," *J. Opt. Soc. Am.*, vol. 70, no. 5, pp. 562–564, May 1980.

[31] Y. H. Wong, R. L. Thomas, and J. J. Pouch, "Subsurface structures of solids by scanning photoacoustic microscopy," *Applied Physics Letters*, vol. 35, no. 5, pp. 368–369, Sep. 1979.

[32] L. D. Favro, P. K. Kuo, J. J. Pouch, and R. L. Thomas, "Photoacoustic microscopy of an integrated circuit," *Applied Physics Letters*, vol. 36, no. 12, pp. 953–954, Jun. 1980.

[33] G. Busse, "Imaging with the optoacoustic effect," *Optics & Laser Technology*, vol. 12, no. 3, pp. 149–154, 1980.
[34] K. Wada, T. Masujima, H. Yoshida, T. Murakami, N. Yata, and H. Imai, "Application of Photoacoustic Microscopy to Analysis of Biological Components in Tissue Sections," *Chemical & Pharmaceutical Bulletin*, vol. 34, no. 4, pp. 1688–1693, 1986.
[35] T. Masujima, Y. Munekane, C. Kawai, H. Yoshida, H. Imai, L. Juing-Yi, and Y. Sato, "Photoacoustic Imaging Immunoassay for Biological Component Microanalysis," in *Photoacoustic and Photothermal Phenomena*, P. D. P. Hess and P. D. J. Pelzl, Eds. Springer Berlin Heidelberg, 1988, pp. 558–560.
[36] K. Maslov, G. Stoica, and L. V. Wang, "In vivo dark-field reflection-mode photoacoustic microscopy," *Optics letters*, vol. 30, no. 6, pp. 625–627, 2005.
[37] K. Maslov, H. F. Zhang, S. Hu, and L. V. Wang, "Optical-resolution photoacoustic microscopy for in vivo imaging of single capillaries," *Optics Letters*, vol. 33, no. 9, pp. 929–31, May 2008.
[38] S. Hu and L. V. Wang, "Optical-Resolution Photoacoustic Microscopy: Auscultation of Biological Systems at the Cellular Level," *Biophysical Journal*, vol. 105, no. 4, pp. 841–847, Aug. 2013.
[39] G. Ku, K. Maslov, L. Li, and L. V. Wang, "Photoacoustic microscopy with 2-micron transverse resolution," *Journal of Biomedical Optics*, vol. 15, no. 2, p. 021302, 2010.
[40] W. Song, W. Zheng, R. Liu, R. Lin, H. Huang, X. Gong, S. Yang, R. Zhang, and L. Song, "Reflection-mode in vivo photoacoustic microscopy with subwavelength lateral resolution," *Biomed. Opt. Express*, vol. 5, no. 12, pp. 4235–4241, Dec. 2014.
[41] F. S. Foster, C. J. Pavlin, K. A. Harasiewicz, D. A. Christopher, and D. H. Turnbull, "Advances in ultrasound biomicroscopy," *Ultrasound in Medicine & Biology*, vol. 26, no. 1, pp. 1–27, Jan. 2000.
[42] C. Zhang, K. Maslov, J. Yao, and L. V. Wang, "In vivo photoacoustic microscopy with 7.6-μm axial resolution using a commercial 125-MHz ultrasonic transducer," *J. Biomed. Opt*, vol. 17, no. 11, pp. 116016–116016, Nov. 2012.
[43] A. Prost, F. Poisson, and E. Bossy, "Photoacoustic generation by a gold nanosphere: From linear to nonlinear thermoelastics in the long-pulse illumination regime," *Phys. Rev. B*, vol. 92, no. 11, p. 115450, Sep. 2015.
[44] JunjieYao and L. V. Wang, "Sensitivity of photoacoustic microscopy," *Photoacoustics*, vol. 2, no. 2, pp. 87–101, 2014.
[45] J. Yao and L. V. Wang, "Photoacoustic microscopy," *Laser & Photonics Reviews*, vol. 7, no. 5, pp. 758–778, Sep. 2013.
[46] K. Maslov, H. F. Zhang, S. Hu, and L. V. Wang, "Optical-resolution confocal photoacoustic microscopy," in *Proceedings of SPIE*, 2008, vol. 6856, p. 68561I–68561I–7.
[47] C. Zhang, K. Maslov, and L. V. Wang, "Subwavelength-resolution label-free photoacoustic microscopy of optical absorption in vivo," *Optics Letters*, vol. 35, no. 19, pp. 3195–3197, Oct. 2010.
[48] Z. Tan, Z. Tang, Y. Wu, Y. Liao, W. Dong, and L. Guo, "Multimodal subcellular imaging with microcavity photoacoustic transducer," *Opt. Express*, vol. 19, no. 3, pp. 2426–2431, Jan. 2011.
[49] Z. Tan, Y. Liao, Y. Wu, Z. Tang, and R. K. Wang, "Photoacoustic microscopy achieved by microcavity synchronous parallel acquisition technique," *Opt. Express, OE*, vol. 20, no. 5, pp. 5802–5808, Feb. 2012.
[50] G. He, B. Li, and S. Yang, "In vivo imaging of a single erythrocyte with high-resolution photoacoustic microscopy," *Front. Optoelectron.*, pp. 1–6, Dec. 2014.
[51] R. L. Shelton, S. P. Mattison, and B. E. Applegate, "Volumetric imaging of erythrocytes using label-free multiphoton photoacoustic microscopy," *J. Biophoton.*, vol. 7, no. 10, pp. 834–840, Oct. 2014.
[52] S. P. Mattison and B. E. Applegate, "Simplified method for ultra high-resolution photoacoustic microscopy via transient absorption," *Optics Letters*, vol. 39, no. 15, p. 4474, Aug. 2014.
[53] R. L. Shelton and B. E. Applegate, "Ultrahigh resolution photoacoustic microscopy via transient absorption," *Biomed. Opt. Express, BOE*, vol. 1, no. 2, pp. 676–686, Sep. 2010.
[54] A. Danielli, K. Maslov, A. Garcia-Uribe, A. M. Winkler, C. Li, L. Wang, Y. Chen, I. Gerald W. Dorn, and L. V. Wang, "Label-free photoacoustic nanoscopy," *J. Biomed. Opt*, vol. 19, no. 8, pp. 086006–086006, 2014.
[55] Z. Xie, S. Chen, T. Ling, L. J. Guo, P. L. Carson, and X. Wang, "Pure optical photoacoustic microscopy," *Optics Express*, vol. 19, no. 10, pp. 13081–13086, 2011.
[56] B. Dong, H. Li, Z. Zhang, K. Zhang, S. Chen, C. Sun, and H. F. Zhang, "Isometric multimodal photoacoustic microscopy based on optically transparent micro-ring ultrasonic detection," *Optica*, vol. 2, no. 2, pp. 169–176, Feb. 2015.
[57] C. Zhang, S. Chen, T. Ling, and L. Jay Guo, "Review of Imprinted Polymer Microrings as Ultrasound Detectors: Design, Fabrication, and Characterization," *IEEE Sensors Journal*, vol. 15, no. 6, pp. 3241–3248, Jun. 2015.
[58] C. Zhang, T. Ling, S.-L. Chen, and L. J. Guo, "Ultrabroad Bandwidth and Highly Sensitive Optical Ultrasonic Detector for Photoacoustic Imaging," *ACS Photonics*, vol. 1, no. 11, pp. 1093–1098, Nov. 2014.
[59] C. G. A. Hoelen, F. F. M. de Mul, R. Pongers, and A. Dekker, "Three-dimensional photoacoustic imaging of blood vessels in tissue," *Optics Letters*, vol. 23, pp. 648–650, Apr. 1998.
[60] W. Shi, P. Hajireza, P. Shao, A. Forbrich, and R. J. Zemp, "In vivo near-realtime volumetric optical-resolution photoacoustic microscopy using a high-repetition-rate nanosecond fiber-laser," *Opt. Express*, vol. 19, no. 18, pp. 17143–17150, 2011.
[61] E. Z. Zhang, J. G. Laufer, R. B. Pedley, and P. C. Beard, "In vivo high-resolution 3D photoacoustic imaging of superficial vascular anatomy," *Phys. Med. Biol.*, vol. 54, no. 4, p. 1035, Feb. 2009.
[62] R. G. M. Kolkman, E. Hondebrink, W. Steenbergen, and F. F. M. de Mul, "In vivo photoacoustic imaging of blood vessels using an extreme-narrow aperture sensor," *IEEE Journal of Selected Topics in Quantum Electronics*, vol. 9, no. 2, pp. 343–346, Mar. 2003.
[63] R. G. M. Kolkman, P. J. Brands, W. Steenbergen, and T. G. van Leeuwen, "Real-time in vivo photoacoustic and ultrasound imaging," *Journal of Biomedical Optics*, vol. 13, no. 5, p. 050510, 2008.
[64] R. G. M. Kolkman, W. Steenbergen, and T. G. van Leeuwen, "In vivo photoacoustic imaging of blood vessels with a pulsed laser diode.," *Lasers in medical science*, vol. 21, no. 3, pp. 134–9, 2006.
[65] S. Hu and L. V. Wang, "Photoacoustic imaging and characterization of the microvasculature," *J. Biomed. Opt*, vol. 15, no. 1, pp. 011101–011101, Jan. 2010.
[66] H. F. Zhang, K. Maslov, M. Sivaramakrishnan, G. Stoica, and L. V. Wang, "Imaging of hemoglobin oxygen saturation variations in single vessels in vivo using photoacoustic microscopy," *Applied Physics Letters*, vol. 90, no. 5, pp. 053901–053901–3, Jan. 2007.
[67] T. I. Karu, "Multiple roles of cytochrome c oxidase in mammalian cells under action of red and IR-A radiation," *IUBMB Life*, vol. 62, no. 8, pp. 607–610, Aug. 2010.
[68] C. Zhang, Y. S. Zhang, D.-K. Yao, Y. Xia, and L. V. Wang, "Label-free photoacoustic microscopy of cytochromes," *J. Biomed. Opt*, vol. 18, no. 2, pp. 020504–020504, Jan. 2013.

[69] Y. Wang, K. Maslov, Y. Zhang, S. Hu, L. Yang, Y. Xia, J. Liu, and L. V. Wang, "Fiber-laser-based photoacoustic microscopy and melanoma cell detection," *Journal of Biomedical Optics*, vol. 16, no. 1, p. 011014, 2011.

[70] J. Yao, "Photoimprint Photoacoustic Microscopy for Three-Dimensional Label-Free Subdiffraction Imaging," *Phys. Rev. Lett.*, vol. 112, no. 1, 2014.

[71] D.-K. Yao, R. Chen, K. Maslov, Q. Zhou, and L. V. Wang, "Optimal ultraviolet wavelength for in vivo photoacoustic imaging of cell nuclei," *Journal of Biomedical Optics*, vol. 17, no. 5, pp. 056004–056004–7, May 2012.

[72] D.-K. Yao, K. Maslov, K. K. Shung, Q. Zhou, and L. V. Wang, "In vivo label-free photoacoustic microscopy of cell nuclei by excitation of DNA and RNA," *Optics Letters*, vol. 35, no. 24, pp. 4139–41, Dec. 2010.

[73] D. Pan, B. Kim, L. V. Wang, and G. M. Lanza, "A brief account of nanoparticle contrast agents for photoacoustic imaging," *Wiley Interdisciplinary Reviews: Nanomedicine and Nanobiotechnology*, vol. 5, no. 6, pp. 517–543, 2013.

[74] J. V. Jokerst and S. S. Gambhir, "Molecular Imaging with Theranostic Nanoparticles," *Acc. Chem. Res.*, vol. 44, no. 10, pp. 1050–1060, Oct. 2011.

[75] C. D. M. F. M. FRCPath, *Diagnostic Histopathology of Tumors*, 4 edition. Philadelphia, PA: Churchill Livingstone, 2013.

[76] Y. S. Zhang, J. Yao, C. Zhang, L. Li, L. V. Wang, and Y. Xia, "Optical-Resolution Photoacoustic Microscopy for Volumetric and Spectral Analysis of Histological and Immunochemical Samples," *Angew. Chem. Int. Ed.*, vol. 53, no. 31, pp. 8099–8103, Jul. 2014.

[77] T. Mosmann, "Rapid colorimetric assay for cellular growth and survival: Application to proliferation and cytotoxicity assays," *Journal of Immunological Methods*, vol. 65, no. 1–2, pp. 55–63, Dec. 1983.

[78] Y. Zhang, X. Cai, Y. Wang, C. Zhang, L. Li, S. Choi, L. V. Wang, and Y. Xia, "Noninvasive Photoacoustic Microscopy of Living Cells in Two and Three Dimensions through Enhancement by a Metabolite Dye," *Angewandte Chemie*, vol. 123, no. 32, pp. 7497–7501, Aug. 2011.

[79] P. K. Jain, K. S. Lee, I. H. El-Sayed, and M. A. El-Sayed, "Calculated Absorption and Scattering Properties of Gold Nanoparticles of Different Size, Shape, and Composition: Applications in Biological Imaging and Biomedicine," *Journal of Physical Chemistry B*, vol. 110, no. 14, pp. 7238–7248, 2006.

[80] S. K. Ghosh and T. Pal, "Interparticle Coupling Effect on the Surface Plasmon Resonance of Gold Nanoparticles: From Theory to Applications," *Chem. Rev.*, vol. 107, no. 11, pp. 4797–4862, Nov. 2007.

[81] E. E. Connor, J. Mwamuka, A. Gole, C. J. Murphy, and M. D. Wyatt, "Gold nanoparticles are taken up by human cells but do not cause acute cytotoxicity.," *Small*, vol. 1, no. 3, pp. 325–7, Mar. 2005.

[82] N. Lewinski, V. Colvin, and R. Drezek, "Cytotoxicity of nanoparticles," *Small*, vol. 4, no. 1, pp. 26–49, Jan. 2008.

[83] K. Sokolov, M. Follen, J. Aaron, I. Pavlova, A. Malpica, R. Lotan, and R. Richards-Kortum, "Real-Time Vital Optical Imaging of Precancer Using Anti-Epidermal Growth Factor Receptor Antibodies Conjugated to Gold Nanoparticles," *Cancer Res*, vol. 63, no. 9, pp. 1999–2004, May 2003.

[84] T. Niidome, M. Yamagata, Y. Okamoto, Y. Akiyama, H. Takahashi, T. Kawano, Y. Katayama, and Y. Niidome, "PEG-modified gold nanorods with a stealth character for in vivo applications," *Journal of Controlled Release*, vol. 114, no. 3, pp. 343–347, Sep. 2006.

[85] D. Peer, J. M. Karp, S. Hong, O. C. Farokhzad, R. Margalit, and R. Langer, "Nanocarriers as an emerging platform for cancer therapy," *Nat Nano*, vol. 2, no. 12, pp. 751–760, Dec. 2007.

[86] L. Brannon-Peppas and J. O. Blanchette, "Nanoparticle and targeted systems for cancer therapy," *Advanced Drug Delivery Reviews*, vol. 64, Supplement, pp. 206–212, Dec. 2012.

[87] K. Cho, X. Wang, S. Nie, Z. (Georgia) Chen, and D. M. Shin, "Therapeutic Nanoparticles for Drug Delivery in Cancer," *Clin Cancer Res*, vol. 14, no. 5, pp. 1310–1316, Mar. 2008.

[88] E. Boisselier and D. Astruc, "Gold nanoparticles in nanomedicine: preparations, imaging, diagnostics, therapies and toxicity," *Chem. Soc. Rev.*, vol. 38, no. 6, pp. 1759–1782, May 2009.

[89] P. Ghosh, G. Han, M. De, C. K. Kim, and V. M. Rotello, "Gold nanoparticles in delivery applications," *Advanced Drug Delivery Reviews*, vol. 60, no. 11, pp. 1307–1315, Aug. 2008.

[90] Y. Wang, X. Xie, X. Wang, G. Ku, K. L. Gill, D. P. O'Neal, G. Stoica, and L. V. Wang, "Photoacoustic Tomography of a Nanoshell Contrast Agent in the in Vivo Rat Brain," *Nano Lett.*, vol. 4, no. 9, pp. 1689–1692, Sep. 2004.

[91] K. Homan, S. Kim, Y.-S. Chen, B. Wang, S. Mallidi, and S. Emelianov, "Prospects of molecular photoacoustic imaging at 1064 nm wavelength," *Opt. Lett.*, vol. 35, no. 15, pp. 2663–2665, Aug. 2010.

[92] S. Mallidi, T. Larson, J. Tam, P. P. Joshi, A. Karpiouk, K. Sokolov, and S. Emelianov, "Multiwavelength Photoacoustic Imaging and Plasmon Resonance Coupling of Gold Nanoparticles for Selective Detection of Cancer," *Nano Letters*, vol. 9, no. 8, pp. 2825–2831, Aug. 2009.

[93] M. Eghtedari, A. Oraevsky, J. a Copland, N. a Kotov, A. Conjusteau, and M. Motamedi, "High sensitivity of in vivo detection of gold nanorods using a laser optoacoustic imaging system," *Nano letters*, vol. 7, no. 7, pp. 1914–8, Jul. 2007.

[94] J.-W. Kim, E. I. Galanzha, E. V. Shashkov, H.-M. Moon, and V. P. Zharov, "Golden carbon nanotubes as multimodal photoacoustic and photothermal high-contrast molecular agents," *Nature Nanotechnology*, vol. 4, no. 10, pp. 688–694, 2009.

[95] G. P. Luke, J. N. Myers, S. Y. Emelianov, and K. V. Sokolov, "Sentinel lymph node biopsy revisited: ultrasound-guided photoacoustic detection of micrometastases using molecularly targeted plasmonic nanosensors," *Cancer Res*, p. canres.0796.2014, Aug. 2014.

[96] Y. S. Zhang, Y. Wang, L. Wang, Y. Wang, X. Cai, C. Zhang, L. V. Wang, and Y. Xia, "Labeling Human Mesenchymal Stem Cells with Gold Nanocages for in vitro and in vivo Tracking by Two-Photon Microscopy and Photoacoustic Microscopy," *Theranostics*, vol. 3, no. 8, pp. 532–543, Jul. 2013.

[97] J. R. Cook, W. Frey, and S. Emelianov, "Quantitative Photoacoustic Imaging of Nanoparticles in Cells and Tissues," *ACS Nano*, vol. 7, no. 2, pp. 1272–1280, Feb. 2013.

[98] S. Yang, F. Ye, and D. Xing, "Intracellular label-free gold nanorods imaging with photoacoustic microscopy," *Optics Express*, vol. 20, no. 9, pp. 10370–10375, Apr. 2012.

[99] W. Bost, F. Stracke, E. C. Weiss, S. Narasimhan, M. C. Kolios, and R. Lemor, "High frequency optoacoustic microscopy," in *Annual International Conference of the IEEE Engineering in Medicine and Biology Society*, 2009, pp. 5883–6.

[100] M. Rui, W. Bost, E. C. Weiss, R. Lemor, and M. C. Kolios, "Photoacoustic Microscopy and Spectroscopy of Individual Red Blood Cells," *International Journal of Radiation Oncology, Biology, Physics*, pp. 3–5, 2010.

[101] M. Rui, S. Narashimhan, W. Bost, F. Stracke, E. Weiss, R. Lemor, and M. C. Kolios, "Gigahertz optoacoustic imaging for cellular imaging," in *Proceedings of SPIE*, 2010, vol. 7564, pp. 756411–756411–6.

[102] W. Bost, F. Stracke, M. Fournelle, and R. Lemor, "Developing a high-resolution photoacoustic microscopy platform," in *4th*

European Conference of the International Federation for Medical and Biological Engineering, 2009, pp. 448–451.

[103] W. Bost, Y. Kohl, F. Stracke, M. Fournelle, and R. Lemor, "High resolution optoacoustic detection of nanoparticles on living cells," in *IEEE Ultrasonics Symposium*, 2009, pp. 120–123.

[104] E. C. Weiss, P. Anastasiadis, G. Pilarczyk, R. M. Lemor, and P. V. Zinin, "Mechanical Properties of Single Cells by High-Frequency Time-Resolved Acoustic Microscopy," *IEEE Transactions on Ultrasonics, Ferroelectrics and Frequency Control*, vol. 54, no. 11, pp. 2257–2271, Nov. 2007.

[105] E. M. Strohm, G. J. Czarnota, and M. C. Kolios, "Quantitative measurements of apoptotic cell properties using acoustic microscopy," *IEEE Transactions on Ultrasonics, Ferroelectrics and Frequency Control*, vol. 57, no. 10, pp. 2293–2304, Oct. 2010.

[106] E. M. Strohm, E. S. L. Berndl, and M. C. Kolios, "High frequency label-free photoacoustic microscopy of single cells," *Photoacoustics*, vol. 1, no. 3–4, pp. 49–53, Dec. 2013.

[107] J. M. M. Pinkerton, "The Absorption of Ultrasonic Waves in Liquids and its Relation to Molecular Constitution," *Proceedings of the Physical Society. Section B*, vol. 62, no. 2, pp. 129–141, Feb. 1949.

[108] E. M. Strohm and M. C. Kolios, "Classification of blood cells and tumor cells using label-free ultrasound and photoacoustics," *Cytometry*, vol. 87, no. 8, pp. 741–749, Aug. 2015.

[109] M. M. Wintrobe, J. P. Greer, and G. R. Lee, *Wintrobe's Clinical Hematology*. Philadelphia: Wolters Kluwer/Lippincott Williams & Wilkins, 2009.

[110] R. W. Horobin and K. J. Walter, "Understanding Romanowsky staining. I: The Romanowsky-Giemsa effect in blood smears," *Histochemistry*, vol. 86, no. 3, pp. 331–336, 1987.

[111] E. M. Strohm, M. J. Moore, and M. C. Kolios, "Ultrasound and photoacoustic imaging of single leukocytes with micrometer resolution," *Submitted*, 2015.

[112] A. K. Loya, J. P. Dumas, and T. Buma, "Photoacoustic microscopy with a tunable source based on cascaded stimulated Raman scattering in a large-mode area photonic crystal fiber," in *IEEE Ultrasonics Symposium*, 2012, pp. 1208–1211.

[113] V. V. Yakovlev, H. F. Zhang, G. D. Noojin, M. L. Denton, R. J. Thomas, and M. O. Scully, "Stimulated Raman photoacoustic imaging," *PNAS*, vol. 107, no. 47, pp. 20335–20339, Nov. 2010.

[114] P. Hajireza, A. Forbrich, and R. Zemp, "In-Vivo functional optical-resolution photoacoustic microscopy with stimulated Raman scattering fiber-laser source," *Biomed Opt Express*, vol. 5, no. 2, pp. 539–546, Jan. 2014.

[115] T. Buma, B. C. Wilkinson, and T. C. Sheehan, "Near-infrared spectroscopic photoacoustic microscopy using a multi-color fiber laser source," *Biomedical Optics Express*, vol. 6, no. 8, p. 2819, Aug. 2015.

[116] X. Wang, Y. Pang, G. Ku, X. Xie, G. Stoica, and L. V. Wang, "Noninvasive laser-induced photoacoustic tomography for structural and functional in vivo imaging of the brain," *Nature Biotechnology*, vol. 21, no. 7, pp. 803–806, 2003.

[117] H. F. Zhang, K. Maslov, G. Stoica, and L. V. Wang, "Functional photoacoustic microscopy for high-resolution and noninvasive in vivo imaging," *Nature Biotechnology*, vol. 24, no. 7, pp. 848–851, 2006.

[118] H. F. Zhang, K. Maslov, and L. V. Wang, "In vivo imaging of subcutaneous structures using functional photoacoustic microscopy," *Nature Protocols*, vol. 2, no. 4, pp. 797–804, Jan. 2007.

[119] V. Ntziachristos and D. Razansky, "Molecular imaging by means of multispectral optoacoustic tomography (MSOT)," *Chem. Rev.*, vol. 110, no. 5, pp. 2783–2794, May 2010.

[120] L. V. Wang and S. Hu, "Photoacoustic Tomography: In Vivo Imaging from Organelles to Organs," *Science*, vol. 335, no. 6075, pp. 1458–1462, Mar. 2012.

[121] J. Yao, L. Wang, J.-M. Yang, K. I. Maslov, T. T. W. Wong, L. Li, C.-H. Huang, J. Zou, and L. V. Wang, "High-speed label-free functional photoacoustic microscopy of mouse brain in action," *Nat Meth*, vol. 12, no. 5, pp. 407–410, May 2015.

[122] D. Razansky, M. Distel, C. Vinegoni, R. Ma, N. Perrimon, R. W. Köster, and V. Ntziachristos, "Multispectral opto-acoustic tomography of deep-seated fluorescent proteins in vivo," *Nat Photon*, vol. 3, no. 7, pp. 412–417, Jul. 2009.

[123] L. Wang, K. Maslov, and L. V. Wang, "Single-cell label-free photoacoustic flowoxigraphy in vivo," *PNAS*, vol. 110, no. 15, pp. 5759–5764, Apr. 2013.

[124] L. Gao, L. Wang, C. Li, Y. Liu, H. Ke, C. Zhang, and L. V. Wang, "Single-cell photoacoustic thermometry," *J. Biomed. Opt*, vol. 18, no. 2, pp. 026003–026003, Feb. 2013.

[125] L. Gao, C. Zhang, C. Li, and L. V. Wang, "Intracellular temperature mapping with fluorescence-assisted photoacoustic-thermometry," *Applied Physics Letters*, vol. 102, no. 19, pp. 193705–193705–5, May 2013.

[126] V. P. Zharov, E. I. Galanzha, Y. Menyaev, and V. V. Tuchin, "In vivo high-speed imaging of individual cells in fast blood flow," *Journal of Biomedical Optics*, vol. 11, no. 5, pp. 054034–054034–4, Sep. 2006.

[127] V. P. Zharov, E. I. Galanzha, E. V. Shashkov, N. G. Khlebtsov, and V. V. Tuchin, "In vivo photoacoustic flow cytometry for monitoring of circulating single cancer cells and contrast agents," *Optics Letters*, vol. 31, no. 24, pp. 3623–3625, Dec. 2006.

[128] V. P. Zharov, E. I. Galanzha, E. V. Shashkov, J.-W. Kim, N. G. Khlebtsov, and V. V. Tuchin, "Photoacoustic flow cytometry: principle and application for real-time detection of circulating single nanoparticles, pathogens, and contrast dyes in vivo," *Journal of Biomedical Optics*, vol. 12, no. 5, pp. 051503–051503–14, Oct. 2007.

[129] E. I. Galanzha, E. V. Shashkov, P. M. Spring, J. Y. Suen, and V. P. Zharov, "In vivo, Noninvasive, Label-Free Detection and Eradication of Circulating Metastatic Melanoma Cells Using Two-Color Photoacoustic Flow Cytometry with a Diode Laser," *Cancer Research*, vol. 69, no. 20, pp. 7926–7934, Oct. 2009.

[130] E. I. Galanzha, E. V. Shashkov, V. V. Tuchin, and V. P. Zharov, "In vivo multispectral, multiparameter, photoacoustic lymph flow cytometry with natural cell focusing, label-free detection and multicolor nanoparticle probes," *Cytometry Part A*, vol. 73A, no. 10, pp. 884–894, Oct. 2008.

[131] D. A. Nedosekin, M. A. Juratli, M. Sarimollaoglu, C. L. Moore, N. J. Rusch, M. S. Smeltzer, V. P. Zharov, and E. I. Galanzha, "Photoacoustic and photothermal detection of circulating tumor cells, bacteria and nanoparticles in cerebrospinal fluid in vivo and ex vivo," *J Biophotonics*, vol. 6, no. 6–7, pp. 523–533, Jun. 2013.

[132] D. A. Nedosekin, M. Sarimollaoglu, E. I. Galanzha, R. Sawant, V. P. Torchilin, V. V. Verkhusha, J. Ma, M. H. Frank, A. S. Biris, and V. P. Zharov, "Synergy of photoacoustic and fluorescence flow cytometry of circulating cells with negative and positive contrasts," *J Biophotonics*, vol. 6, no. 5, pp. 425–434, May 2013.

[133] V. P. Zharov, "Ultrasharp nonlinear photothermal and photoacoustic resonances and holes beyond the spectral limit," *Nature Photonics*, no. January, pp. 1–7, Jan. 2011.

[134] E. I. Galanzha and V. P. Zharov, "Photoacoustic flow cytometry," *Methods*, vol. 57, no. 3, pp. 280–296, Jul. 2012.

[135] M. A. Juratli, M. Sarimollaoglu, D. A. Nedosekin, A. V. Melerzanov, V. P. Zharov, and E. I. Galanzha, "Dynamic

Fluctuation of Circulating Tumor Cells during Cancer Progression," *Cancers*, vol. 6, no. 1, pp. 128–142, Jan. 2014.

[136] M. A. Juratli, M. Sarimollaoglu, E. Siegel, D. A. Nedosekin, E. Galanzha, J. Y. Suen, and V. P. Zharov, "Real-time monitoring of circulating tumor-cell release during tumor manipulation using in vivo photoacoustic and fluorescent flow cytometry," *Head Neck*, Aug. 2013.

[137] E. I. Galanzha and V. P. Zharov, "Circulating Tumor Cell Detection and Capture by Photoacoustic Flow Cytometry in Vivo and ex Vivo," *Cancers*, vol. 5, no. 4, pp. 1691–1738, Dec. 2013.

[138] V. V. Tuchin, A. Tárnok, and V. P. Zharov, "In vivo flow cytometry: a horizon of opportunities," *Cytometry A*, vol. 79, no. 10, pp. 737–745, Oct. 2011.

[139] X. Hu, C.-W. Wei, J. Xia, I. Pelivanov, M. O'Donnell, and X. Gao, "Trapping and Photoacoustic Detection of CTCs at the Single Cell per Milliliter Level with Magneto-Optical Coupled Nanoparticles," *Small*, vol. 9, no. 12, pp. 2046–2052, 2013.

[140] C. M. O'Brien, K. D. Rood, K. Bhattacharyya, T. DeSouza, S. Sengupta, S. K. Gupta, J. D. Mosley, B. S. Goldschmidt, N. Sharma, and J. A. Viator, "Capture of circulating tumor cells using photoacoustic flowmetry and two phase flow," *Journal of Biomedical Optics*, vol. 17, no. 6, pp. 061221–061221–9, May 2012.

[141] R. M. Weight and J. A. Viator, "Detection of Circulating Tumor Cells by Photoacoustic Flowmetry," in *Molecular Diagnostics for Melanoma*, M. Thurin and F. M. Marincola, Eds. Humana Press, 2014, pp. 655–663.

[142] Z. Xie, S. Jiao, H. F. Zhang, and C. A. Puliafito, "Laser-scanning optical-resolution photoacoustic microscopy," *Optics Letters*, vol. 34, no. 12, pp. 1771–1773, Jun. 2009.

[143] H. Fang and L. V. Wang, "M-mode photoacoustic particle flow imaging," *Optics letters*, vol. 34, no. 5, pp. 671–3, Mar. 2009.

[144] R. K. Saha and M. C. Kolios, "A simulation study on photoacoustic signals from red blood cells," *The Journal of the Acoustical Society of America*, vol. 129, no. 5, p. 2935, 2011.

[145] K. Kim, Z. Wang, and S.-H. Ha, "Photoacoustic design parameter optimization for deep tissue imaging by numerical simulation," pp. 822346–822346, Feb. 2012.

[146] Z. Wang, S. Ha, and K. Kim, "Evaluation of finite-element-based simulation model of photoacoustics in biological tissues," in *Proceedings of SPIE*, 2012, vol. 8320, p. 83201L–83201L–9.

[147] E. M. Strohm, Elizabeth S.L. Berndl, and M. C. Kolios, "Probing red blood cell morphology using high frequency photoacoustics," *Biophysical Journal*, vol. 105, no. 1, pp. 59–67, Jul. 2013.

[148] E. M. Strohm, I. Gorelikov, N. Matsuura, and M. C. Kolios, "Modeling photoacoustic spectral features of micron-sized particles," *Phys. Med. Biol.*, vol. 59, no. 19, pp. 5795–5810, Oct. 2014.

[149] A. Needles, A. Heinmiller, J. Sun, C. Theodoropoulos, D. Bates, D. Hirson, M. Yin, and F. S. Foster, "Development and initial application of a fully integrated photoacoustic micro-ultrasound system," *IEEE Transactions on Ultrasonics, Ferroelectrics and Frequency Control*, vol. 60, no. 5, pp. 888–897, 2013.

[150] H. Ke, T. N. Erpelding, L. Jankovic, C. Liu, and L. V. Wang, "Performance characterization of an integrated ultrasound, photoacoustic, and thermoacoustic imaging system," *Journal of Biomedical Optics*, vol. 17, no. 5, pp. 056010–056010–6, May 2012.

[151] R. A. Kruger, P. Liu, Y. "'Richard'" Fang, and C. R. Appledorn, "Photoacoustic ultrasound (PAUS)—Reconstruction tomography," *Medical Physics*, vol. 22, no. 10, pp. 1605–1609, Oct. 1995.

[152] C. Kim, T. N. Erpelding, L. Jankovic, M. D. Pashley, and L. V. Wang, "Deeply penetrating in vivo photoacoustic imaging using a clinical ultrasound array system," *Biomedical Optics Express*, vol. 1, no. 1, p. 278, Aug. 2010.

[153] T. Harrison, J. C. Ranasinghesagara, H. Lu, K. Mathewson, A. Walsh, and R. J. Zemp, "Combined photoacoustic and ultrasound biomicroscopy," *Optics Express*, vol. 17, no. 24, pp. 22041–22046, 2009.

[154] C.-W. Wei, T.-M. Nguyen, J. Xia, B. Arnal, E. Y. Wong, I. M. Pelivanov, and M. O'Donnell, "Real-time integrated photoacoustic and ultrasound (PAUS) imaging system to guide interventional procedures: ex vivo study," *IEEE Transactions on Ultrasonics, Ferroelectrics, and Frequency Control*, vol. 62, no. 2, pp. 319–328, Feb. 2015.

[155] K. Pantel, R. H. Brakenhoff, and B. Brandt, "Detection, clinical relevance and specific biological properties of disseminating tumour cells," *Nature Reviews Cancer*, vol. 8, no. 5, pp. 329–340, May 2008.

[156] C. Alix-Panabières and K. Pantel, "Circulating Tumor Cells: Liquid Biopsy of Cancer," *Clinical Chemistry*, vol. 59, no. 1, pp. 110–118, Jan. 2013.

[157] S. Nagrath, L. V. Sequist, S. Maheswaran, D. W. Bell, D. Irimia, L. Ulkus, M. R. Smith, E. L. Kwak, S. Digumarthy, A. Muzikansky, P. Ryan, U. J. Balis, R. G. Tompkins, D. A. Haber, and M. Toner, "Isolation of rare circulating tumour cells in cancer patients by microchip technology," *Nature*, vol. 450, no. 7173, pp. 1235–1239, Dec. 2007.

[158] V. C. Anderson, "Sound Scattering from a Fluid Sphere," *The Journal of the Acoustical Society of America*, vol. 22, no. 4, p. 426, 1950.

[159] J. Faran, "Sound scattering by solid cylinders and spheres," *The Journal of the Acoustical Society of America*, vol. 23, no. 4, pp. 405–418, 1951.

[160] R. Hickling, "Analysis of echoes from a solid elastic sphere in water," *Journal of the Acoustical Society of America*, vol. 34, no. 10, pp. 1582–1592, 1962.

[161] R. K. Johnson, "Sound scattering from a fluid sphere revisited," *The Journal of the Acoustical Society of America*, vol. 61, no. 2, p. 375, 1977.

[162] G. Gaunaurd, "Elastic and acoustic resonance wave scattering," *Applied Mechanics Reviews*, vol. 42, no. 6, pp. 143–168, 1989.

[163] G. P. Downey, D. E. Doherty, B. Schwab, E. L. Elson, P. M. Henson, and G. S. Worthen, "Retention of leukocytes in capillaries: role of cell size and deformability," *Journal of Applied Physiology*, vol. 69, no. 5, pp. 1767–1778, Nov. 1990.

[164] E. M. Strohm, B. Moon, D. H. Hwang, S. H. Tsai, and M. C. Kolios, "Development of a microfluidic device with integrated high frequency ultrasound probe for particle characterization," in *IEEE International Ultrasonics Symposium*, Chicago, USA, 2014.

Eric M. Strohm received his B.Sc. degree in Physics from McMaster University in 1999. From 2002-2007, he was employed as a member of research staff at the Xerox Research Centre of Canada. He received his M.Sc. degree in 2009 and Ph.D. degree in 2013 in Biomedical Physics from Ryerson University. He is currently a Postdoctoral Fellow in the Biomedical Ultrasound Laboratory at Ryerson University. His research interests include ultrasound and photoacoustic imaging and spectroscopy, photonics, nanotechnology, and microfluidics for the characterization of biological cells and tissues.

Michael J. Moore received his B. Math degree in Mathematical Physics from the University of Waterloo, Ontario, Canada, in 2013. He is currently pursuing his Ph.D. degree at Ryerson University,

Ontario, Canada, in the CAMPEP Accredited Biomedical Physics program. His research interests include acoustic microscopy, photoacoustic microscopy, and high-frequency quantitative photoacoustics of single biological cells.

Michael C. Kolios is a Professor in the Department of Physics at Ryerson University and associate Dean of Research and Graduate Studies in the Faculty of Science. His work focuses on the use of ultrasound and optics in the biomedical sciences. He has published 73 peer-reviewed journal publications, 5 book chapters, and 96 papers in conference proceedings. He has been invited to speak at 35 different organizations or conferences, and has been the keynote and plenary speaker for conferences in Canada, India and China. He has received numerous teaching and research awards, including the Canada Research Chair in Biomedical Applications of Ultrasound and the Ontario Premier's Research Excellence Award. He is on the editorial board of the journals Ultrasound Imaging and Photoacoustics and is member of many national and international committees, including the IEEE International Ultrasonics Symposium Technical Program Committee. He is a member of the National Institutes of Health (NIH) Biomedical Imaging Technology A study section and was previously a member of the Canadian Institutes of Health Research (CIHR) Medical Physics and Imaging (MPI) panel.